Integrated Self-Powered Sensors Based on 2D Material Devices

Ziwei Huo, Yichen Wei, Yifei Wang, Zhong Lin Wang,* and Qijun Sun*

With the development of the Internet of Things, there is an increasing need for clean energy and large-scale sensory systems. Triboelectric/piezoelectric nanogenerators (TENGs/PENGs), have attracted considerable attention as a new type of power generation terminal, which can harvest surrounding energy and convert it into electrical energy. To improve the output performance of nanogenerators (NGs) and diversify related applications, 2D materials with high carrier mobility and excellent piezoelectric properties can be directly used or integrated as different types of self-powered sensors. In this review, the authors first introduce the excellent piezoelectric and optoelectronic properties of 2D materials, followed by the triboelectric series of 2D materials used in TENGs. The categories of integrated self-powered sensors based on 2D materials are then summarized according to their different structures and compositions. We also discuss in detail the recent applications of integrated self-powered sensors based on 2D materials from five aspects. Finally, the challenges and outlooks in the research field of self-powered sensors are featured. Given the continuous development of self-powered sensors based on 2D materials, they are considered to have significant potential for applications in biomedicine, environmental detection, human motion monitoring, energy harvesting, and smart wearable devices.

1. Introduction

With the rapid and continuous development of the current economy and technology, traditional energy supply is facing an increasingly serious shortage. The continuous exploitation and utilization of fossil fuels have caused serious harm to the human living environment. Therefore, the development and utilization of new energy have become an important issue that must be solved in the development of human society.[1] The development and utilization of renewable energy have attracted more and more attention, especially in these countries with energy shortages. Some common renewable clean energy such as solar energy, wind energy, and ocean energy has been successfully collected and converted into electricity. However, these energy conversion devices are mainly based on electromagnetic conversion or photovoltaic effect, and the manufacture and maintenance of these devices will consume a large amount of manpower and financial resources.[2,3] In this context, nanogenerators (NGs) have been applied due to their low cost, zero power consumption, environmental friendliness, and strong stability.[4,5]

Recently, the Internet of Things (IoT), as the core of the worldwide information industry, has been rapidly developed. The pursuit of high integration, simple, portable, and easy commercialization has prompted the application of sensors in life.[6] With the development of IoT, it also faces more and more challenges in the technical field. As an indispensable part, sensors have become the biggest obstacle to the development of the IoT. As the traditional energy source of sensors, although the power consumption of each unit can be reduced to the microwatt level, the total power consumption is amazing when forming large-scale network applications, which not only affects the sensor life but also brings environmental pollution.[7] In this regard, scientists try to solve this problem with the self-powered sensor based on NGs, which can work continuously without an external power supply. The electrical signal generated by triboelectric/piezoelectric nanogenerators (TENGs/PENGs) can be readily used as both the energy source of the sensor and the output signal detected by the sensor, which has been intensively investigated as self-powered sensors themselves or integrated into self-powered systems.[8–10]

Z. Huo, Y. Wei, Y. Wang, Z. L. Wang, Q. Sun
Beijing Institute of Nanoenergy and Nanosystems
Chinese Academy of Sciences
Beijing 101400, P. R. China
E-mail: sunqijun@binn.cas.cn

Z. Huo, Y. Wei, Y. Wang, Z. L. Wang, Q. Sun
School of Nanoscience and Technology
University of Chinese Academy of Sciences
Beijing 100049, P. R. China

Y. Wei, Q. Sun
Center on Nanoenergy Research
School of Physical Science and Technology
Guangxi University
Nanning 530004, P. R. China

Z. L. Wang
School of Materials Science and Engineering
Georgia Institute of Technology
Atlanta, GA 30332, USA
E-mail: zlwang@gatech.edu

Q. Sun
Shandong Zhongke Naneng Energy Technology Co., Ltd.
Dongying 257061, P. R. China

The ORCID identification number(s) for the author(s) of this article can be found under https://doi.org/10.1002/adfm.202206900.

**ADVANCED
SCIENCE NEWS**

www.advancedsciencenews.com

**ADVANCED
FUNCTIONAL
MATERIALS**

www.afm-journal.de

Successful exfoliation of graphene (Gr) has inspired intensive research on the 2D material family.[11] In recent years, related 2D materials have attracted the attention of scholars due to their unique characteristics and functions. Specifically, Wang et al. proved the piezoelectric properties of 2D van der Waals semiconductor MoS_2 via experiment and introduced the concept of piezotronics/piezo-phototronics into the 2D field for the first time.[12] As is known, due to the large internal resistance of TENG and special materials required for PENG, the total output power of the device is limited to a certain extent.[13] The excellent properties[14] and high carrier mobility[15,16] of 2D materials can just make up for this problem. 2D materials have also attracted much attention due to their advantages of effectively regulatable charge transport inside the material and improved charge carrier mobility. Therefore, the integration of NGs and 2D materials with fantastic properties can not only improve the energy conversion efficiency but also diversify relevant applications, which can be better used in energy harvesting and self-powered systems. Cai et al. reported a TENG sensor based on graphene oxide composite films, which could efficiently collect external low-frequency mechanical energy and convert it into electrical energy. Furthermore, when the load resistance of the device is 400 MΩ, the power density of the sensor can reach 31.36 W m^{-2}.[17] Wang et al. reported a TENG-driven MXene-based self-powered sensor with a good response to NO_2 at room temperature, which had potential applications in environmental monitoring.[18]

Here, we introduce in detail, the integrated self-powered sensors based on 2D materials (**Figure 1**). First, we discuss the typical piezoelectric and optoelectronic properties of 2D materials, followed by the triboelectric series of 2D materials used in TENG devices. Then, TENG/PENG self-powered sensors based on different 2D materials are introduced in detail. These 2D materials are graphene, graphene-like, transition metal dichalcogenides (TMDs), main group metal dichalcogenides (MDCs), alloys, and heterostructures. Finally, we further discuss the applications of TENG/PENG self-powered sensors based on 2D materials in different fields: human motion monitoring, energy harvesting, biomedical engineering, environmental monitoring, Artificial Intelligence (AI), and neuromorphic devices.

2. Characteristics of 2D Materials for Self-Powered Sensors

Following the footprint of 1D materials, the successful exfoliation of a single atomic layer of graphene marked the birth of 2D materials in 2004.[19] The thickness of 2D materials is only a single or few atoms thick (typically less than several nanometers), while electrons can move freely in two dimensions. Besides, the carrier migration and heat diffusion are confined in 2D plane, 2D materials exhibit greatly compelling properties.[20] The structures and types of the 2D materials are greatly abundant, including elemental 2D materials represented by graphene, graphene-like materials represented by MXene, and hexagonal boron nitride (h-BN), TMDs represented by MoS_2, MDCs, alloys, heterostructures, and other 2D materials. The section mainly reviews the piezoelectric and photoelectric properties of 2D materials used in nanogenerators derived self-powered sensors as well as the triboelectric series of 2D materials.

2.1. Piezoelectric Properties

The piezoelectric effect was first discovered by French physicists P. and J. Curie in 1880. When weight was placed on a quartz crystal, an electric charge proportional to the pressure is generated on the crystal surface. Thus, there are positive and negative charges on the two opposite surfaces of the crystal to form a voltage, which is defined as the piezoelectric effect. Since the appearance of piezoelectric materials, they gradually became an important part of the material field due to their unique properties. Traditional piezoelectric materials mainly include inorganic piezoelectric crystals (e.g., quartz crystals), piezoelectric ceramics (e.g., barium titanate), and organic piezoelectric polymers (e.g., polyvinylidene fluoride). With the development of electronics, piezoelectric materials are often used in various sensors and energy converters. These traditional piezoelectric materials are often ignored due to the interaction between electric fields and carriers. Wang et al. successfully constructed the PENG with ZnO nanowires, for the first time proving that semiconductor materials with a certain concentration of carriers can still maintain significant intrinsic piezoelectric properties.[12] Piezotronics and piezo-phototronics were proposed in subsequent studies.

Graphene is composed of the most stable six-membered carbon ring, which is connected one by one as basic units. The carbon atom hybridizes in sp^2 mode and contributes an electron to the remaining p-orbital, eventually forming a large π-state where electrons can move freely between atoms. The structure with an asymmetry is a necessary condition for piezoelectric properties of materials. Therefore, graphene does not
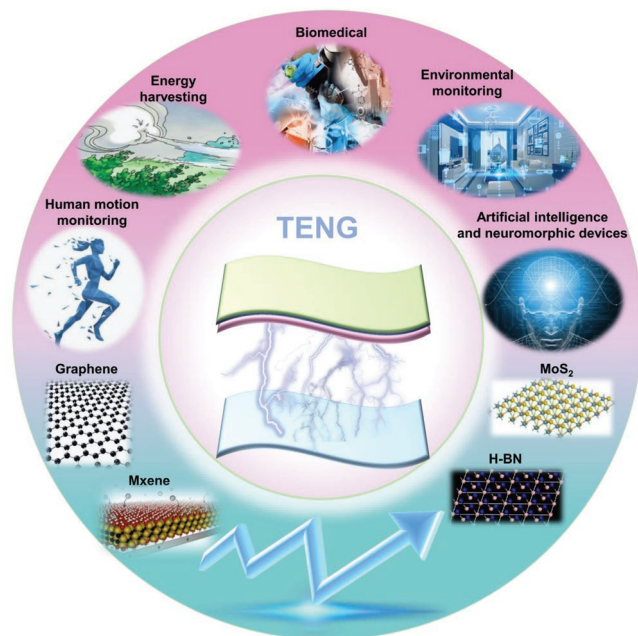

Figure 1. Application of self-powered NG sensors based on 2D materials.

**ADVANCED
SCIENCE NEWS**

www.advancedsciencenews.com

**ADVANCED
FUNCTIONAL
MATERIALS**

www.afm-journal.de

have a piezoelectric effect. However, by properly manipulating the structure and introducing asymmetric centers, it can produce piezoelectric properties. The piezoelectric properties of 2D graphene are usually achieved by surface modification engineering or structural control engineering. Xu et al. reported the positive piezoelectric effect of multilayer graphene films deposited on Si/SiO₂ substrates with etched grooves after mechanical exfoliation.[21] **Figure 2**a depicts the optical microscope image of a suspended bilayer graphene device (left) and the setup schematic of pressure-modulated conductance microscopy (PCM, right) that performs piezoelectric measurements on a suspended graphene device. After exerting pressure on the device, the opposite charges will be generated on the relative surfaces as the deformation occurs, and the mechanical energy will be converted into electrical energy. When the external pressure is removed and the deformation disappears, the device will return to its uncharged state again.

h-BN and MXene, as 2D graphene-like materials, were found to have piezoelectric properties. Figure 2b shows that h-BN consists of equal numbers of boron and nitrogen atoms arranged in a hexagonal structure within each layer. The boron and nitrogen atoms are bound by covalent bonds, while these layers stack together by the weak van der Waals interaction.[22] PAINE et al. synthesized the h-BN and proved it was an attractive ceramic material with good piezoelectric properties by experiments.[23] MXene is a new kind of 2D material with a graphene-like structure.[24] The MXene is produced by selective etching of the precursor MAX phases with a general formula of $M_{n+1}AX_n$ (n = 1, 2, 3), where M is the transition metal element (Ti, Sc, Zr, Nb, etc.), A is another element from group IIIA or IVA (Al, Si, Sn, In, etc.), and X is carbon or/and nitrogen. The precursor MAX phase of MXene is a kind of ternary layered compound with excellent properties of both ceramic and metal.[25] Tan et al. reported piezotronic effect of monolayer MXene for nanogenerators and piezotronics.[26] Figure 2c shows the deformation of MXene hexagon structure in tensile state leads to piezoelectric polarization and piezoelectric field. Notably, under the typical piezotronic effect of MXene material, the current changes under positive bias and negative bias are asymmetric, that is, the piezoelectric potential is asymmetric to the Schottky barrier height modulation.

In addition, TMDs represented by MoS₂ also have excellent piezoelectric properties.[14] TMDs have a general chemical formula: MX₂. M is the transition metals, including IV_B (Ti, Zr), V_B (V, Nb, Ta), and VI_B (Mo, W); X is chalcogenides element, including S, Se, and Te. Wu et al. confirmed the theoretical prediction that monolayer MoS₂ has strong piezoelectricity. The coupling of mechanical and piezoelectrical properties enables it as nano-scale devices to be used for sensing and energy harvesting.[27] Han et al. reported a high-performance PENG based on MoS₂ nanosheets.[28] Figure 2d shows the schematic illustration of the PENG based on MoS₂, composed of monolayer MoS₂ nanosheet and Au electrodes on polyethylene terephthalate (PET) substrate. By reducing the carrier concentration of MoS₂, the shielding effect of free carriers on piezoelectric polarized charge can be prevented. The maximum power of PENG based on monolayer MoS₂ nanosheet increased by ≈10 times. Zhu et al. reported the piezoelectricity of free-standing monolayer MoS₂.[29] As shown in Figure 2e, a monolayer of MoS₂ is superimposed by S–Mo–S unit cell with a thickness of 0.6 nm (left), and the Mo atom is in the center (middle left). Viewing from the top (middle right), each unit cell (shaded in yellow) consists of two S atoms occupying the same site in the hexagonal lattice, and the Mo atom locates on the opposite site, thus breaking the mirror symmetry in the x–y-plane but preserving in the z-direction. When the external electric field is directed from the S to Mo (right), the unit cell is elongated, resulting in compressive stress in the x-direction and tensile stress in the y-direction. In addition to TMDs, other 2D MDCs (such as SnSe, GeS, SnS, GaSe, GaS, and InSe) and transition metal oxides (SnO₂ and MoO₂) also have a good piezoelectric effect.[30] Chang et al. reported piezoelectric properties of SnSe monolayer grown on graphene.[31] Figure 2f shows the schematic illustration of ferroelectric switching achieved by applying bias voltage pulse (V_P) at a point on the graphene substrate close to the SnSe monolayer nanosheet. Manjula et al. reported the simple and flexible PENG based on 2D ZnO nanosheet networks. As shown in Figure 2g, the 2D ZnO nanosheets bend under external force and generate piezopotential. Negative and positive potentials are induced in the compressed and stretched states of the nanosheets, respectively.

2.2. Photoelectric Properties

The photoelectric effect was put forward by Hertz in 1887 when he discovered that light irradiation on certain substances could cause changes in their electrical properties. Einstein proposed the photon hypothesis and successfully explained the photoelectric effect according to the phenomenon of electrons emitted from metal surfaces under the influence of light in 1905. Due to the structural advantages of 2D materials, researchers have gradually focused on their optical properties. The variation of the optical properties of 2D materials with the number of layers can be detected by various optical methods, such as optical contrast spectrum, Rayleigh scattering, Raman spectrum, light absorption spectrum, photoinduced spectrum, second harmonic generation, etc. With the increased layers of 2D materials, the peaks, intensity, and linewidth in the spectra may change significantly, or some new optical features may appear. Until now, various 2D materials have been fabricated with remarkable optoelectronic characteristics, e.g., unique optical nonlinearities, readily tunable light-matter interaction, and ultrafast photo response from ultraviolet to radio waves. As is known, the principle of the optoelectronic properties of 2D materials for electroluminescence is to utilize the injection of electrons and holes in devices with p-n junction or Schottky junction to recombine in the junction region to generate electroluminescence. A strong local electric field is formed from the n-region of the positively charged region to the p-region of the negatively charged region in the junction. In contrast, when the p-n junction or Schottky junction is illuminated, photogenerated electrons and holes will move directionally under the local electric field of the junction, resulting in a photocurrent.[32,33] Accordingly, the photodetectors based on p-n junction or Schottky junction exploit the built-in potential present in the junction to achieve efficient separation and fast transfer of photogenerated carriers, which enables them to detect optical
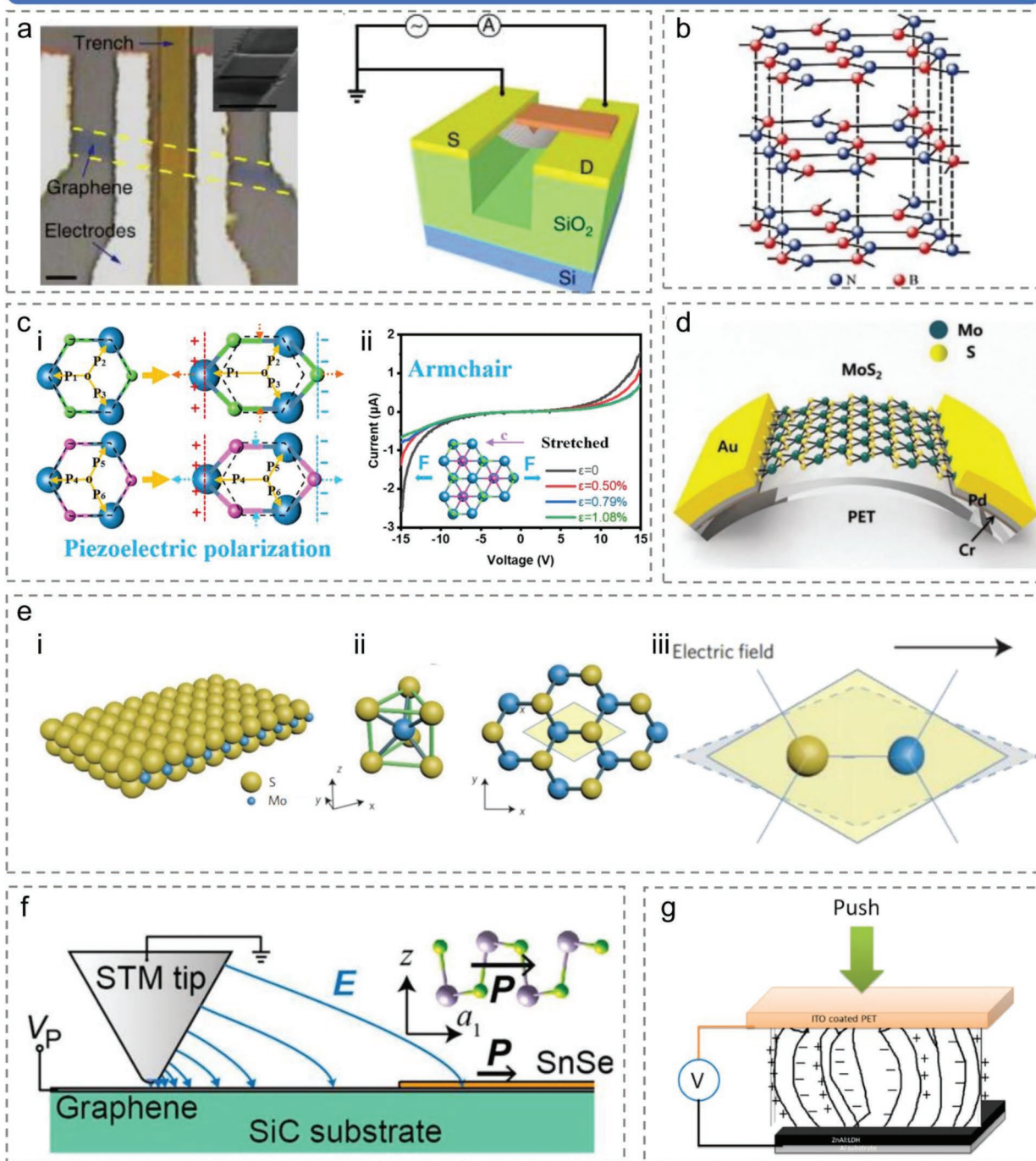
Figure 2. Piezoelectric properties of 2D materials for self-powered sensors used in NGs. a) SEM image of a bilayer graphene device(left) and the schematic of the piezoconductive measurements on graphene devices (right). Reproduced under terms of the CC-BY license.[21] Copyright 2015, The Authors, published by Springer Nature. b) Crystal structure of the h-BN. c), i) The tensile deformation of the simplified T_x-T_i hexagonal structure (upper) and T_i-C hexagonal structure (lower). ii) The characteristics of the piezoelectric effect in the $Ti_3C_2T_x$ MXene. Reproduced with permission.[26] Copyright 2021, Elsevier Ltd. d) Schematic of the PNG based on monolayer MoS_2 nanosheets. Reproduced with permission.[28] Copyright 2018, Wiley-VCH GmbH. e), i) A single layer of MoS_2 consists of S–Mo–S stacking with a total thickness of 0.6 nm, ii) with the Mo atom centered in the trigonal prism, each unit cell consists of two S atoms, with the Mo atom residing in the opposite site. iii) With an external electric field pointing from the S site to the Mo site, the unit cell is elongated, resulting in compressive stress in the x direction and tensile stress in the y direction. Reproduced with permission.[29] Copyright 2014, Springer Nature. f) Schematic diagram of the realization of ferroelectric switching by SnSe monolayer on the graphene substrate. Reproduced with permission.[31] Copyright 2020, Nano Letters. g) Proposed mechanism for the piezo voltage generation. Reproduced with permission.[201] Copyright 2020, Elsevier B.V.

**ADVANCED
SCIENCE NEWS**

www.advancedsciencenews.com

**ADVANCED
FUNCTIONAL
MATERIALS**

www.afm-journal.de

signals without an external bias voltage.[34,35] 2D materials have unique optoelectronic properties of direct bandgap electronic structure and strong exciton effect, which make them have unique electrical and photonic performance and great potential in the field of self-powered sensors with p-n junction, Schottky junction, and photoelectrochemical structures.[36]

Graphene is a 2D material that can transfer electrons faster than any known conductor at room temperature. As a semiconductor material with zero band gap, graphene has excellent carrier mobility and special transport characteristics,[37–39] which has wide application in photovoltaic cells, photovoltaic power generation, photodetectors, and other fields.[40,41] Graphene has excellent optical properties and a wide absorption wavelength. Its absorption rate is ≈2.3% over a wide wavelength range, which is almost transparent. Within a certain range, the absorption rate increases by 2.3% with each additional layer thickness of graphene (**Figure 3**a). The red and green lines are the ideal Dirac Fermion curve and theoretical calculation curve respectively, and the gray area is the standard deviation from the calculation result. With a rarely low-energy electronic structure, graphene also has excellent optical properties. The optical absorption of graphene mainly depends on the interbond transition (Figure 3bi). Photogenerated carriers form thermal Fermi-Dirac distribution under the action of hot carriers, reaching thermal equilibrium (Figure 3bii). At high excitation intensity, it causes the edges of the conduction band and valence band to be filled, which hinders further absorption (Figure 3biii). As a graphene-like material, h-BN also has excellent optical properties.[42] Satawara et al. reported a visible-blind ultraviolet detector based on h-BN.[43] Figure 3c shows that h-BN is transparent material in the visible region. Its absorption and reflection only occur in the ultraviolet region. The reflectivity is low in the infrared region and high in the ultraviolet region.

TMDs have been widely used in electric and optoelectronic devices due to their semiconductor properties and high absorption coefficients in the spectral range.[44] Hieu et al. studied the optical properties of MoS_2 by density functional theory (DFT) method.[45] The comparison of refractive index between monolayer and bulk MoS_2 shows that monolayer MoS_2 has high photoluminescence intensity and high photoelectron-hole pair recombination efficiency, which is suitable for optoelectronic devices (Figure 3d). Sayan Roy et al. reported a mid-infrared modulator with high modulation depth in a wide spectrum by changing the carrier density of MoS_2.[46] 2D monolayer WS_2 has also found to have great photoelectric properties.[47–49] Figure 3e shows the introduction of monolayer WS_2 and α-Si on the basis of bulk WS_2 structure, which improves the band structure and optical performance and increases the efficiency of device by more than 23%.[50] 2D ZnO, the representative material of MDCs, has excellent optical properties due to its wide band gap and high exciton binding energy.[51–53] In recent years, the continuous emergence of 2D materials with different physical properties has led to the rise of another new class of materials, namely 2D heterostructure materials. Wang et al. reported the photoelectric conversion properties of 2D ZnO, graphene, Si, Gr/ZnO, Gr/Si, and ZnO/Gr/Si heterostructures.[54] The absorption coefficient of ZnO/Gr/Si remains high over a wide energy range and reaches the maximum in the visible light range (Figure 3fi). The 2D ZnO/Gr/Si vdW heterostructure has high light absorption efficiency and can stably absorb photon energy in a wide frequency range, resulting in more photo-generated electrons and holes, which is beneficial to improving the photoelectric conversion efficiency (Figure 3fii). Huang et al. successfully prepared the WSe_2-MoS_2 heterostructure (Figure 3g) with high-quality planar heterointerface by physical vapor transfer method,[55] and found that the photoluminescence properties of the heterostructure were higher than that of the single material.

2.3. Triboelectric Series of 2D Materials

2D materials have a wide application prospect in the field of ultra-thin solid lubrication at the molecular level due to their ultra-high mechanical strength and extremely low nano friction properties. Among NGs that convert mechanical energy into electricity, TENGs are the most popular.[56] Although people have a certain understanding of the friction properties of graphene-based 2D materials, how to systematically understand the microscopic friction mechanism of such new materials with only a few atomic layers of thickness, and how to regulate and utilize its friction behavior has become a hot topic.[57–59] Kim et al. for the first time reported the TENG using graphene as a friction material in 2014.[60] They prepared graphene-based TENGs (Gr-TENGs) using large-scale graphene grown on copper (Cu) and nickel (Ni) by chemical vapor deposition (CVD) to obtain electrical energy from mechanical stress through graphene. At the same time, the work function of graphene was improved by increasing the number of graphene layers, thus the output performance of TENG was improved. The discovery of excellent tribological properties of 2D materials has further stimulated people's enthusiasm for the study of their friction behavior, and the triboelectrification behavior and mechanism of 2D materials have been reported successively.[61] Minsu Seol et al. reported a sliding TENG structure[62] in which the triboelectric series of MoS_2 was first obtained by rubbing MoS_2 with six different materials (PTFE, PDMS, PC, PET, Mica, Nylon) (**Figure 4**a). The triboelectrification characteristics of MoS_2 are between PTFE and PDMS. In addition, the triboelectrification properties of other 2D materials ($MoSe_2$, WS_2, WSe_2, GR, GO, $AuCl_3$-doped MoS_2, benzyl viologen (BV)-doped MoS_2) are tested by the same method. In order to determine the exact order of other 2D materials in the triboelectric series, the TENG output values based on the electrification between Nylon and target materials are compared. Nylon is a typical positively-charged material in the triboelectric sequence, while other 2D materials are evaluated to exhibit negatively-charged properties (Figure 4b).

3. Self-Powered TENG/PENG Sensors Based on Various 2D Materials

In recent years, as a new type of mechanical energy conversion technology, TENG/PENG has obvious advantages in self-powered sensors/electronics, micro/nano energy sources, distributed high-entropy energy harvesting, and other fields
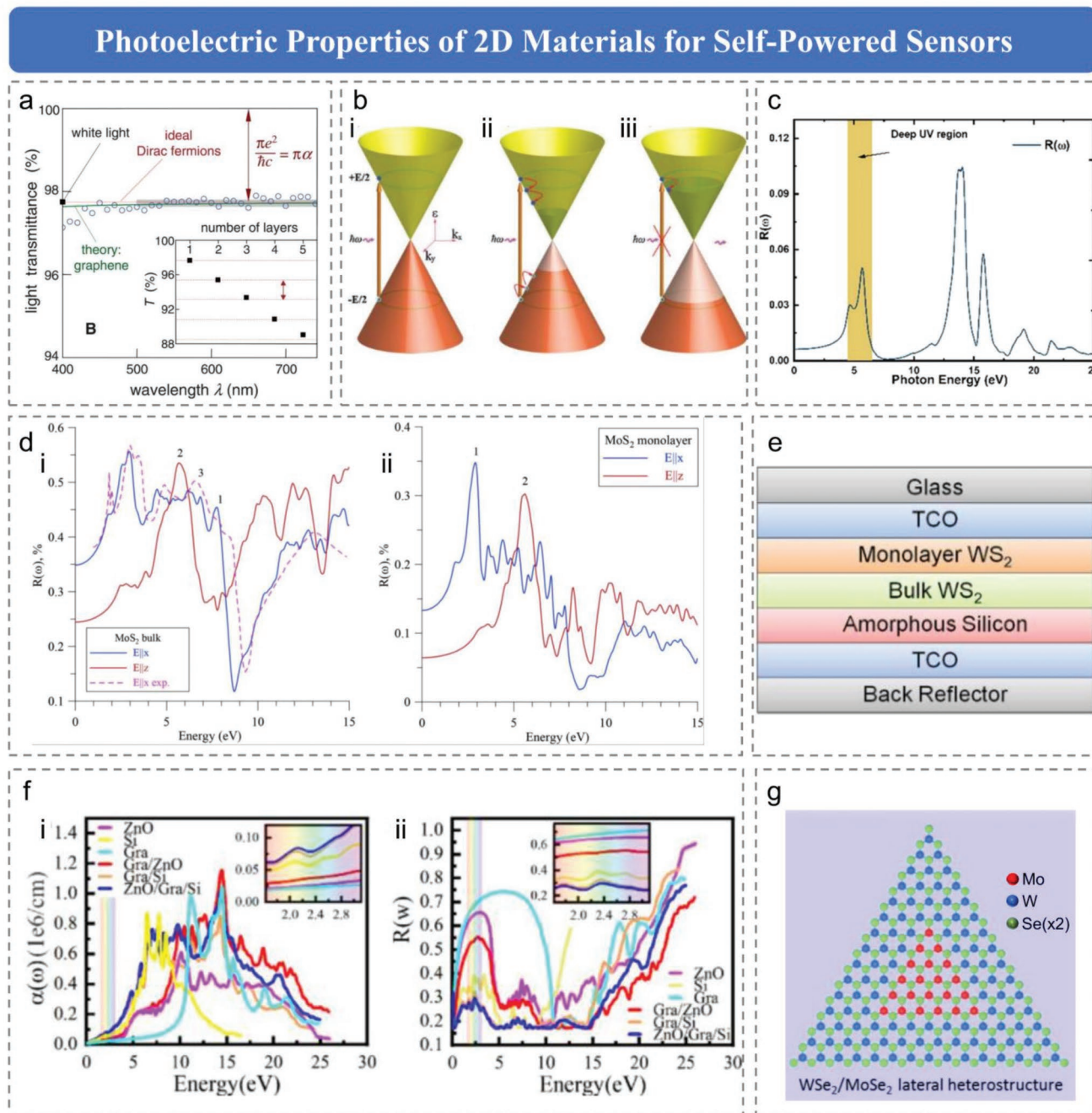
Figure 3. Photoelectric properties of 2D materials for self-powered sensors used in NGs. a) Transmittance spectrum of graphene over a range of photon energies E from near-infrared to violet. Reproduced with permission.[202] Copyright 2008, American Association for the Advancement of Science. b), i) Schematic excitation process responsible for absorption of light in graphene, ii) the photogenerated carriers thermalize and cool down within subpicoseconds to form a hot Fermi-Dirac distribution and iii) the photogenerated carriers block further absorption at high excitation intensity(right). Reproduced with permission.[203] Copyright 2009, Wiley-VCH GmbH. c) Reflectivity R(x) of h-BN. Reproduced with permission.[43] Copyright 2020, Elsevier Ltd. d) Optical reflectivity R(ω) of i) bulk and ii) monolayer MoS2. Reproduced with permission.[45] Copyright 2018, Elsevier Ltd. e) Device structure. Reproduced with permission.[50] Copyright 2017, Elsevier B.V. f), i) Absorption coefficient, ii) reflectivity of 2D ZnO, Gra, Si, Gra/ZnO, Gra/Si, and ZnO/Gra/Si. Reproduced with permission.[54] Copyright 2022, Elsevier Ltd. g) Schematic illustration of the epitaxial lateral heterostructures. Reproduced with permission.[55] Copyright 2014, Nature Publishing Group.

closely related to contact electrification. Compared with traditional materials, 2D materials have become the most potential materials for technical applications due to unique piezoelectric, photoelectric, and mechanical properties. There have been

many reports about TENG/PENG based on 2D materials.[63–71] This part mainly reviews the self-powered TENG/PENG sensors based on the following 2D materials: graphene, graphene-like, TMDs, MDCs, alloys and heterostructures, etc.
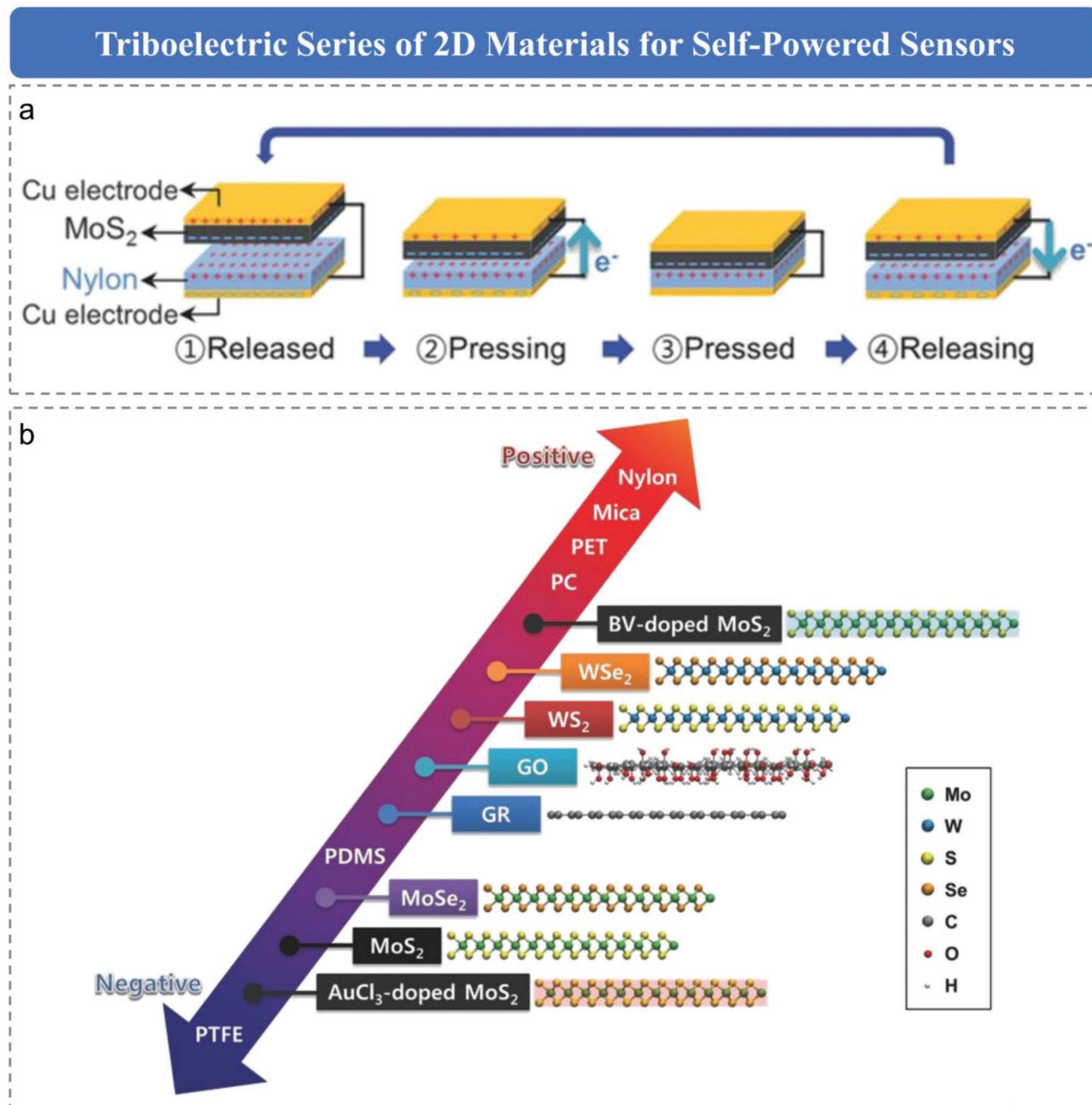
Figure 4. Triboelectric series of 2D Materials. a) Schematic showing the device structure and working principle of the MoS_2–nylon TENG. Reproduced with permission.[62] Copyright 2018, Wiley-VCH GmbH. b) Modified triboelectric series including 2D materials. The molecular structure is shown on the right of the corresponding material. Reproduced with permission.[62] Copyright 2018, Wiley-VCH GmbH.

3.1. Self-Powered Sensors Based on Graphene

Graphene is the earliest 2D material discovered, in which the carbon atoms are arranged in a hexagonal lattice. It is the thinnest and strongest material, which laid a foundation for subsequent research on 2D materials. Taisuke Ohta et al. report that each carbon atom has four valence electrons, the carbon atom in graphene is sp^2 hybrid, so each carbon atom contributes a residual p-electron.[72] The remaining valence electrons form

a large π–bond, which is perpendicular to the plane, forming bonding orbitals π and anti-bonding orbitals π^*, and forming the valence band and conduction band of graphene. Therefore, the Fermi surface of graphene is located at the intersection of valence band and conduction band (**Figure 5**a).

Graphene has good flexibility and is one of the ideal materials for flexible energy storage devices. Xia et al. reported a self-powered measurement-control system by combining flexible pressure sensor based on reduced graphene oxide (rGO)-cloth
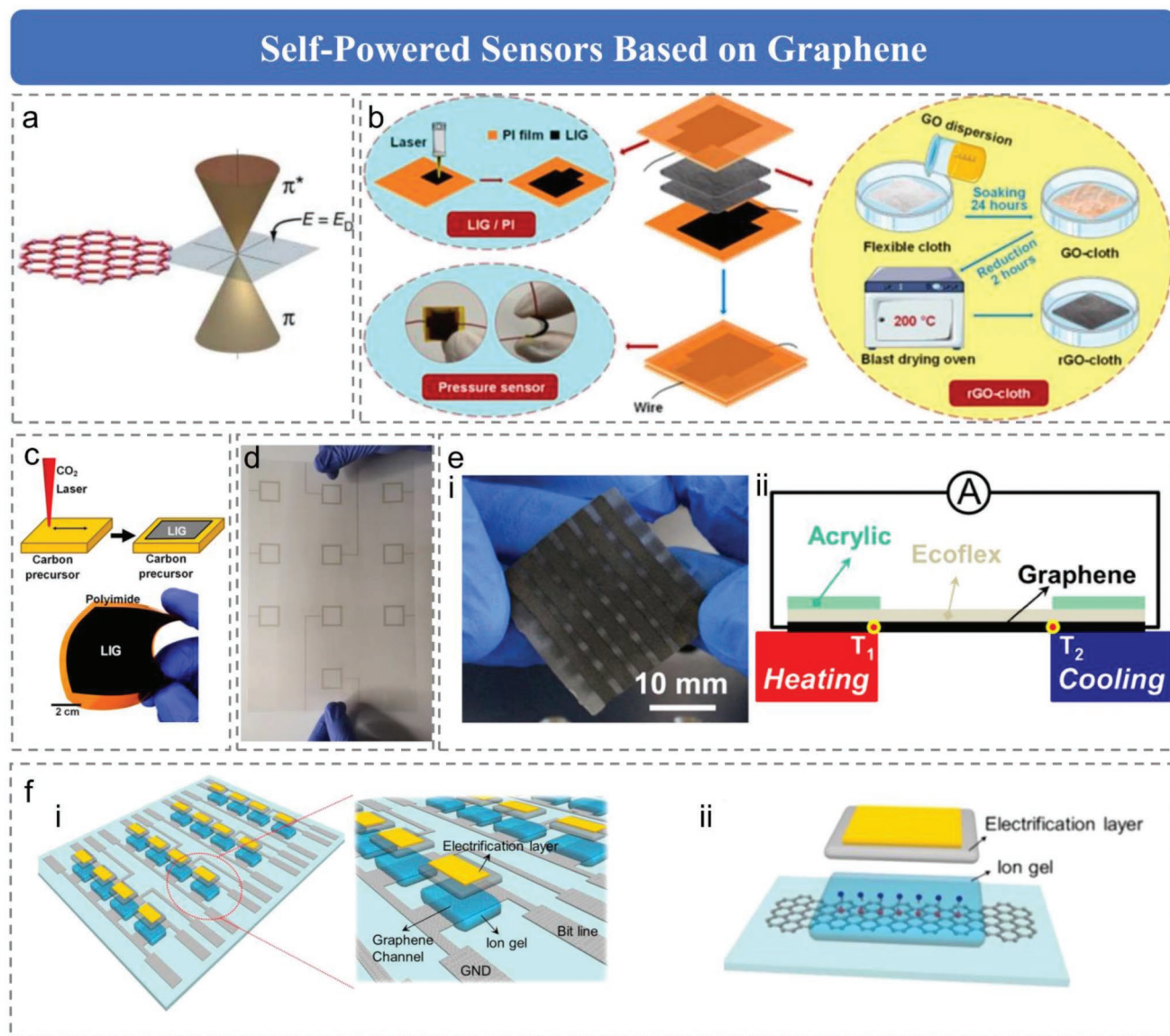
Figure 5. Self-powered NG sensors based on graphene materials. a) Electronic structure of a single layer of graphene. Reproduced with permission.[72] Copyright 2014, American Association for the Advancement of Science. b) Schematic diagrams and photos of rGO-cloth/LIG pressure sensor. The preparation process of LIG/PI, rGO-cloth, and pressure sensor is displayed. Reproduced with permission.[73] Copyright 2022, Elsevier Ltd. c) Schematic for lasing a carbon precursor to synthesize LIG and the optical image of LIG on PI, which demonstrates the flexibility of the films. Reproduced with permission.[74] Copyright 2019, American Chemical Society. d) Photograph of the fabricated TSS device consisting of ten sensor units. Reproduced with permission.[75] Copyright 2019, Wiley-VCH GmbH. e), i) Photographs of a multi-channel 3D strain sensor under original conditions and ii) the schematic diagram showing the structure of stretchable thermoelectric device based on graphene-ecoflex nanocomposite film (right). Reproduced with permission.[76] Copyright 2018, Elsevier Ltd. f), i) Schematic illustration of the mechanosensation-active matrix based on a tribotronic planar graphene transistor array. ii) Schematic illustration of the triboelectric GFET with ion gel as friction layer. Reproduced with permission.[83] Copyright 2018, American Chemical Society.

and laser-induced graphene (LIG)/Nylon TENG on polyimide (PI) substrate, which can detect tiny dynamic signals, and has great applications in the future development of wearable devices, electronic skin, etc. (Figure 5b)[73] The designed sensor can be folded and bent with good flexibility. G. Stanford reported a highly conductive LIG composite with PI which can be used to fabricate TENG sensors with good mechanical bending and contact properties.[74] Charge transfer will occur during the process of contact and separation between LIG/PI

and Al (or LIG/cork and PI), thus causing charge movement in the external circuit (Figure 5c). Tang et al. reported the flexible non-contact TENG sensor for the first time, providing a non-contact design concept for the next generation of touch-screen sensors.[75] The whole device consists of 10 sensing units, in which the top layer, intermediate layer, and bottom layer of each sensing unit are graphene, ITO PET dielectric substrates, respectively (Figure 5d). The device is flexible, transparent, and small size, which can be easily integrated into the smart

**ADVANCED
SCIENCE NEWS**
www.advancedsciencenews.com

**ADVANCED
FUNCTIONAL
MATERIALS**
www.afm-journal.de

electronic screen. It has made a breakthrough in the field of human-computer interaction.

Due to high thermal conductivity and negative thermal expansion coefficient, graphene can be used in thermal interface engineering research. The study of its thermal properties is gradually becoming an important branch of graphene-based self-powered sensors. Zhang et al. reported a multi-channel 3D self-powered ultrasensitive strain sensor system[76] based on graphene and ecoflex thermoelectric composite films (Figure 5ei). The system combines the good thermoelectric properties of graphene and the tensile properties of ecoflex elastomer. It can accurately detect the subtle movements of the human body and achieve the sensing measurement range of high sensitivity, high resolution, and long cycle life. Figure 5eii describes that two parallel-connected Peltier thermoelectric modules are used to establish the thermal gradient difference to study the thermoelectric properties of graphene-ecoflex nanocomposite films. The sensitivity of the sensor can be further adjusted through the temperature difference, so as to achieve high sensitivity.

It is well known that graphene has a strong field effect and extremely high carrier mobility, and its current density is six orders of magnitude higher than that of copper[77–82]. Due to its unparalleled electrical properties, graphene has always been the focus of research. Meng et al. reported for the first time a direct-contact-mode mechanosensing active matrix[83] based on tribotronic planar graphene transistor arrays (4 × 4 graphene field effect transistors (GFETs) with planar geometry) (Figure 5fi, single tribotronic GFET in the matrix is shown in Figure 5fii). Ion gel in graphene transistors was used as the dielectric medium and triboelectrification layer, which could be well coupled with the triboelectric potential to achieve efficient gating and sensory properties. The part of graphene in contact with the ion gel acts as the transistor channel, while the rest constitutes the layout lines and source drain. Different metals or polymers can be used as the positive or negative friction layer materials against the ion-gel dielectrics, outputting different signals and thereby constructing a material recognition sensor. The sensing performance can be effectively regulated by the triboelectric potential gating through the ion gel (dielectric/triboelectric layer). The experimental results show that, the designed tribotronic GFET has higher electrical performance compared with separated coupling of TENG and GFET. The mechanosensation matrix prototype is valuable and instructive for the future development of skin-inspired electronic systems.

3.2. Self-Powered Sensors Based on Graphene-like Materials

Since the first report of MXene ($Ti_3C_2T_x$, where T represents the terminal of the surface, including OH, O, or F) in 2011, a variety of MXene materials has been prepared successively in the laboratory.[25,84–89] As shown in **Figure 6**a, MXene is a graphene-like structure obtained by MAX phase processing. Since M–X has strong bond energy and A is more chemically active, A can be removed from the MAX phase by etching to obtain a 2D structure-MXene similar to graphene.[90] Experiments and studies have shown that such materials have excellent mechanical, electrical, optical, and electrochemical properties.[91–93]

Recently, MXenes have attracted interest in gas sensing due to their remarkable features such as graphene-like morphology, comparable metallic electrical conductivity, large surface-to-volume ratio, mechanical flexibility, and excellent affinity. Wang et al. reported a self-powered NH_3 sensor fabricated from $Ti_3C_2T_x$ MXene and metal-organic framework-derived CuO,[94] which was driven by contact-separation-mode TENG based on PTFE and latex (Figure 6b). The self-powered NH_3 sensor driven by TENG exhibits a good response at room temperature, while TENG can achieve a maximum peak power density of 0.84 W m^{-2} and can illuminate at least 480 LEDs. MXene is not only widely used in the field of gas sensors, but its excellent electrical properties are also often used in the research of other types of self-powered sensors. 2D MXene is a class of conductive material that is more triboelectrically negative than PTFE or Teflon.[95] Cao et al. reported a strain sensor based on wrinkled MXene thin film,[96] in which MXene was brushed onto a latex substrate to improve the tensile properties and surface roughness of the film. As shown in Figure 6c, in order to verify the performance of the conductive layer of the MXene film in the TENG sensor application, the human hand was used as the positive electrode of the friction layer, and the MXene film was used as the negative electrode and conductive layer of the friction layer. In terms of strain sensing, the wrinkled MXene film is demonstrated to have good sensitivity and cycle stability.

The invention of TENG is a landmark discovery in the field of electromechanics and self-powered sensing. In terms of energy conversion and energy harvesting, TENG has its unique advantages.[97–99] There have been many reports on energy conversion and energy harvesting devices based on 2D materials. Figure 6d depicts a highly electronegative and conductive TENG sensor based on MXene material, which can harvest energy from human muscle movement and efficiently convert mechanical energy into electrical energy. MXene not only has the electronegativity induced by the -F group similar to PTFE but also can break the limitation of electrodes and realize the dual-electrode working mode, which provides a wider range of TENG self-powered sensors based on MXene. As shown in Figure 6e, MXene composited nanofibers serve as friction layers for TENG sensors to improve triboelectric energy harvesting efficiency. The dielectric modulation of PVDF by 2D MXene nanosheets increases the dielectric constant and surface charge density of the entire device by 270% and 80%, respectively. Figure 6f shows a highly flexible and efficient TENG sensor based on MXene and PDMS composite film. Using LIG as the electrode of the device and introducing MXene with conductivity and electronegativity into PDMS to prepare porous films can not only improve the conductivity but also improve the tribo-electronegativity.

3.3. Self-Powered Sensors Based on TMDs

MoS_2 is the most typical and important 2D material among TMDs. TMDs can display metallic, semi-metallic, and semiconducting behaviors depending on the polytype and the band structure. MoS_2 is a typical van der Waals material with semiconducting properties.[100–103] MoS_2 has a lower off-current and high on/off ratio and has wider applications in semiconductor

ADVANCED
SCIENCE NEWS
www.advancedsciencenews.com

ADVANCED
FUNCTIONAL
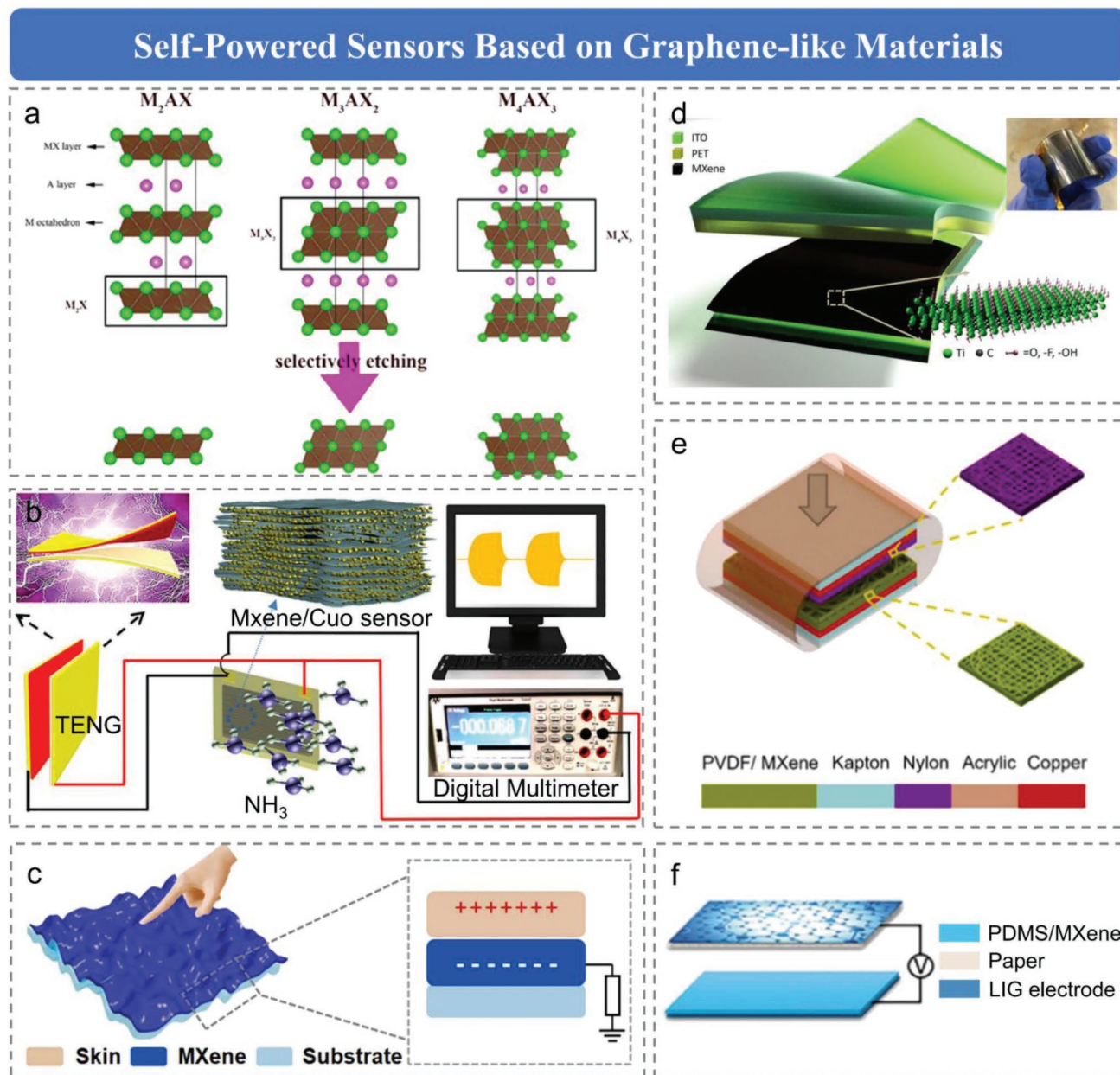**MATERIALS**
www.afm-journal.de

Figure 6. Self-powered NG sensors based on graphene-like materials. a) Crystal structure of MAX phase and corresponding MXene after selectively etching. Reproduced with permission.[90] Copyright 2017, Elsevier Ltd. b) Schematic illustration of self-powered NH_3 sensor driven by TENG. Reproduced with permission.[94] Copyright 2021, American Chemical Society. c) Schematic diagram of the self-powered sensor and the single electrode mode. Reproduced with permission.[96] Copyright 2021, Elsevier Ltd. d) The whole device of the MXene-based TENG sensor. Reproduced with permission.[204] Copyright 2017, Elsevier Ltd. e) The schematic diagram and an optical photograph of the as-fabricated TENG. Reproduced with permission.[205] Copyright 2020, Elsevier Ltd. f) Schematic diagram of Mxene-based TENG self-powered sensor. Reproduced with permission.[206] Copyright 2019, Elsevier Ltd.

devices. In addition, MoS_2 can realize the regulation of the band gap by adsorbing different molecules, and its special layered structure makes it have unique physical properties in photoluminescence and light absorption.[104–106]

Recently, the intrinsic charge accumulation and transport properties of MoS_2 have become the focus of research. Maity et al. reported an ultrasensitive PENG based on composite nanofibers which could be readily tuned with the content of 2D

MoS_2 nanosheets in PVDF.[107] **Figure 7**a depicts the fabrication process of MoS_2-PVDF composite nanofibers. As is known, monolayer MoS_2 consists of three layers of S–Mo–S atoms, in which each S atom and three Mo atoms are combined by covalent bonds, and each Mo atom is combined with six S atoms by covalent bonds. Strong planar chemical bonds ensure the structural stability of MoS_2 (top left). In this work, few-layer MoS_2 nanosheets can be obtained by saline exfoliation of MoS_2
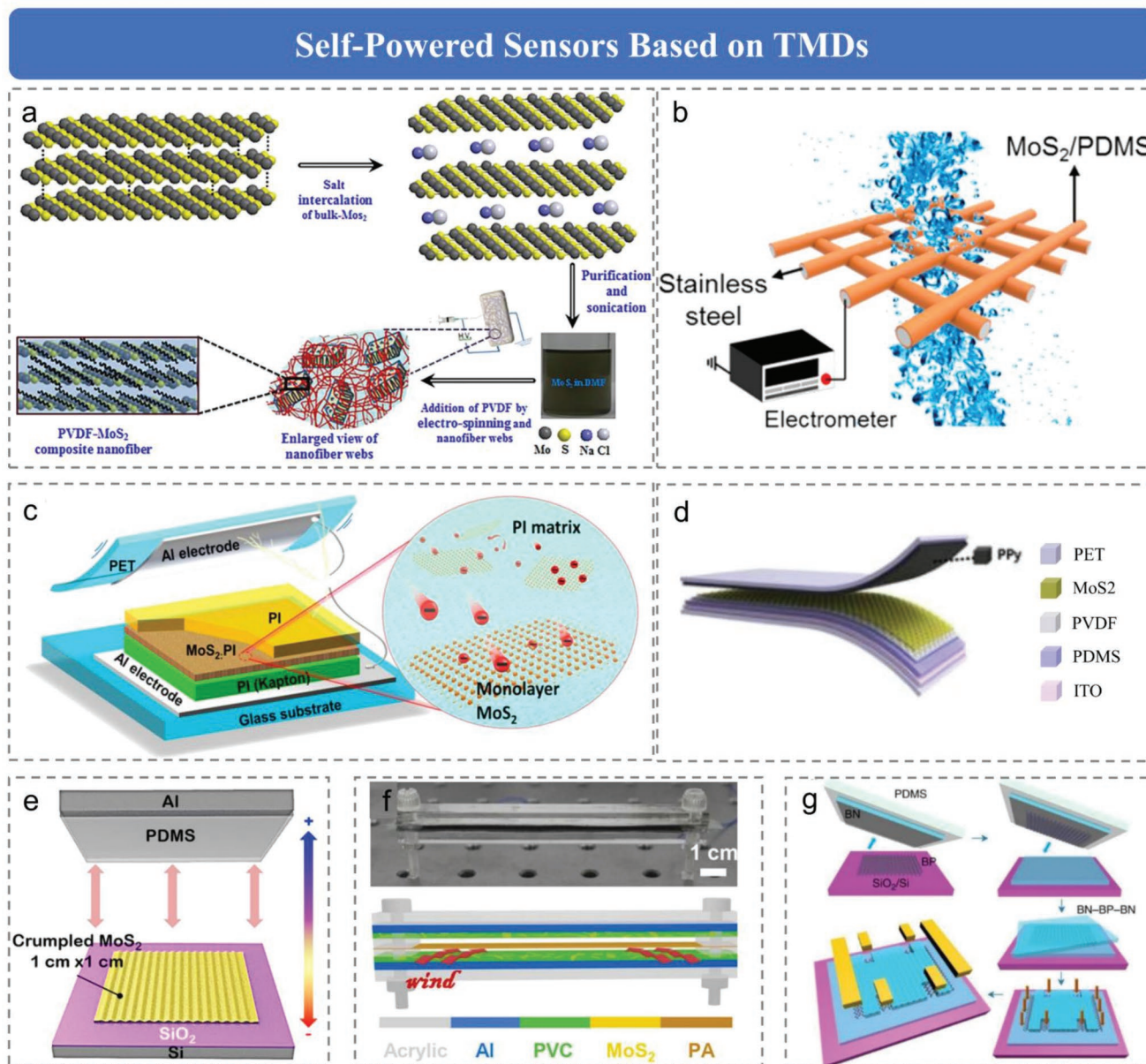
Figure 7. Self-powered NG sensors based on TMDs materials. a) Schematic representation of MoS$_2$ nanosheets dispersed in DMF and the preparation of the PVDF-MoS$_2$ composite nanofiber. Reproduced with permission.[107] Copyright 2017, Wiley-VCH GmbH. b) Illustration of the MoS$_2$/PDMS nanocomposite coating on a commercial stainless steel grid to harvest water flow energy. Reproduced with permission.[108] Copyright 2016, Elsevier Ltd. c) Illustration of the vertical contact-separation mode TENG with a MoS2-monolayer film. The right panel shows a schematic diagram of the electron transfer from the PI layer to the MoS$_2$ monolayer. Reproduced with permission.[109] Copyright 2017, American Chemical Society. d) Schematics of MoS$_2$-based TENG sensor. Reproduced with permission.[110] Copyright 2019, Elsevier Ltd. e) Illustration of MoS$_2$-based TENG device structures. Reproduced with permission.[111] Copyright 2020, Elsevier Ltd. f) A physical photograph of the fabricated TENG. Reproduced with permission.[112] Copyright 2021, Elsevier Ltd. g) Schematic of the BN–BP–BN heterostructure device fabrication process. Reproduced under terms of the CC-BY license.[117] Copyright 2015, The Authors, published by Springer Nature.

powder, and then composite nanofibers can be obtained by electrospun in PVDF stock solution (right). As shown in Figure 7b, Lin et al. reported a self-powered piezoelectric catalytic purification system based on MoS$_2$/PDMS nanocomposite coating.[108] MoS$_2$/PDMS composites were uniformly coated on metal grids and cleaned with acetone, isopropanol, and deionized water. The MoS$_2$ structure has abundant monolayers and odd layers, which is the key components to enhance the piezoelectric

catalytic effect. It is reported that self-powered piezoelectric catalytic system can degrade organic pollutants in wastewater and collect hydromechanical energy from water of different sources.

2D monolayer MoS$_2$ can be used as electron acceptors due to a large specific surface area and quantum confinement effect. Wu et al. reported an enhanced TENG based on MoS$_2$ monolayer nanocomposites acting as electron-acceptor layers.[109] Figure 7c shows the vertical contact-separation-mode TENG

**ADVANCED
SCIENCE NEWS**

www.advancedsciencenews.com

**ADVANCED
FUNCTIONAL
MATERIALS**

www.afm-journal.de

based on monolayer MoS_2. Inset shows a schematic diagram of electron transfer from the PI layer to MoS_2 monolayer. As the electron acceptor in the TENG device, the monolayer MoS_2 can efficiently capture electrons and significantly improve the output performance of the whole device. Kim et al. reported a flexible and bendable TENG self-powered sensor based on MoS_2 due to its remarkable mechanical properties.[110] Figure 7d shows the TENG sensor with a p-n junction structure based on polypyrrole/MoS_2 p-n junction (MoS_2 with a direct band gap of 1.8–1.9 eV). The reported TENG exhibits good rectification behavior, which can improve the output performance.

To investigate the triboelectrification properties of 2D TMDs nanomaterials, Park et al. reported a method to synthesize atomically thin 2D MoS_2 layers by direct one-step laser processing with controlled morphology using a photonic thermal decomposition mechanism. This direct-image-based laser synthesis method in a non-vacuum environment can tune the surface topography of 2D MoS_2 without any additional processing and modification.[111] As Figure 7e illustrated, MoS_2 in different surface morphologies paired with PDMS counter friction material is used to study the TENG devices in contact-separation mode. Zhao et al. reported a TENG self-powered sensor based on PVC/MoS_2 composite film, which has the characteristics of high-performance and long-cycle-life and can be used for wind energy scavenging.[112] Figure 7f depicts the structure of the TENG, in which PVC/MoS_2 composite films and polyamide (PA) films were used as triboelectric materials, and aluminum (Al) sheets with nanostructures were used as electrodes. The excellent lubrication properties of MoS_2 can effectively improve the surface charge density of the composite structure and the wear resistance of the device, and thus improve the life and output performance of the TENG. Similar to the structure of TMDs, atomically thin black phosphorus (BP) has also attracted interest due to its high theoretical mobility, tunable direct band gap and unique bipolar properties, and has potential applications in electronic and optoelectronic devices.[113–116] Chen et al. reported the formation of stable BN-BP-BN heterostructure by encapsulating BP with h-BN.[117] Figure 7g shows the fabrication process of BN–BP–BN heterostructure device with potential self-powered sensing capacities. It provides important clues for the practical application of BP-based nanoelectronic devices. 2D TMDs nanomaterials are widely considered as next-generation electronic materials, and also energy materials, for future flexible, transparent, and wearable electronics and self-powered systems.

3.4. Self-Powered Sensors Based on MDCs

MDCs (SnSe, SnS, ZnS, etc.) have attracted more and more attention due to broadband gaps, excellent optoelectronic properties, and wide application prospects.[118] SnS is a semiconductor with a layered structure, the Sn and S atoms connect to each other by strong chemical bonding in each layer, while these layers stack together thorugh the weak van der Waals interaction.[119] **Figure 8**a shows the cross-sectional crystal structures of SnS along the armchair direction with different stacking sequences: non-centrosymmetric AA and centrosymmetric AB staking (left). Besides, the top view of crystal structure of

monolayer SnS shows biaxiality along the armchair direction. The highlighted area shows thermodynamically stable facets (right).

As the most representative material among MDCs, ZnS has excellent acoustoelectric and photoconductive properties, and can be used in a variety of applications. Besides, ZnS nanostructures can be synthesized by a simple low-temperature hydrothermal method without additional electrode deposition.[120] ZnS nanostructures are very easy to grow on large-area substrates, which are conducive to large-scale production. Qian et al. reported a flexible and high-performance TENG based on ZnS/ZnO nanosheets,[121] the structure of which device is shown in Figure 8b. ZnS/ZnO nanosheets were prepared by a simple method and then combined with PDMS as the friction layer material of TENG. Ultrathin ZnS/ZnO nanosheets can provide a larger contact area, and significantly improve the charge transfer efficiency and output performance.

Mishra et al. reported a TENG self-powered sensor based on 2D ZnS nanosheets.[122] As shown in Figure 8c, the introduction of ZnS nanosheets on the Al substrate increases the surface area and roughness of the device. The self-powered sensors based on 2D ZnS have been proven to drive low-power electronic devices such as digital watches, thermometers, calculators, and 64 LEDs. Gupta et al. reported an efficient energy-harvesting sensor based on ZnS nanosheets, which could harvest biomechanical energy for next-generation flexible self-powered electronic devices.[123] Figure 8d shows the structure of the self-powered TENG sensor. The ITO-coated PET film was covered on the surface of ZnS nanosheets, with a Schottky barrier formed between ZnS and ITO electrode interfaces to facilitate charge transfer.

In addition to chalcogenides, metal oxides have also made a lot of research progress in 2D materials. Gupta et al. reported a high-performance PENG based on 2D vanadium (V)-doped ZnO nanosheets.[124] Figure 8e shows the growth mechanism of V-doped ZnO. The seed layer was deposited on a bare ITO/PET substrate by spin coating. V(OH)$_4^-$ ions are connected at the Zn$^+$ terminated surface, which blocks the 1D growth of V-doped ZnO (bottom middle). Through vanadium doping, the vertically aligned ZnO nanorods were completely transformed into 2D nanosheets, and the obtained 2D morphology could be regarded as nanosheet network. The fabricated ZnO PENG doped with vanadium exhibits ferroelectric behavior, charge inversion phenomenon, and high output performance.

3.5. Self-Powered Sensors Based on Alloys and Heterostructures

2D alloys and heterojunctions make full use of the nano-scale advantages of 2D materials in the vertical direction, showing great application potential and scientific research value for electronics and optoelectronics.[125–127] 2D material heterostructures refer to heterojunctions formed by the close packing of two or more different 2D materials, or the composite structures formed by the close contact between 2D materials and other nanomaterials. The two or more materials that constitute the heterostructure have different band gaps, electrical properties, doping types, optical absorption and luminescence, dielectric constant, work function, etc. The electronic or optoelectronic
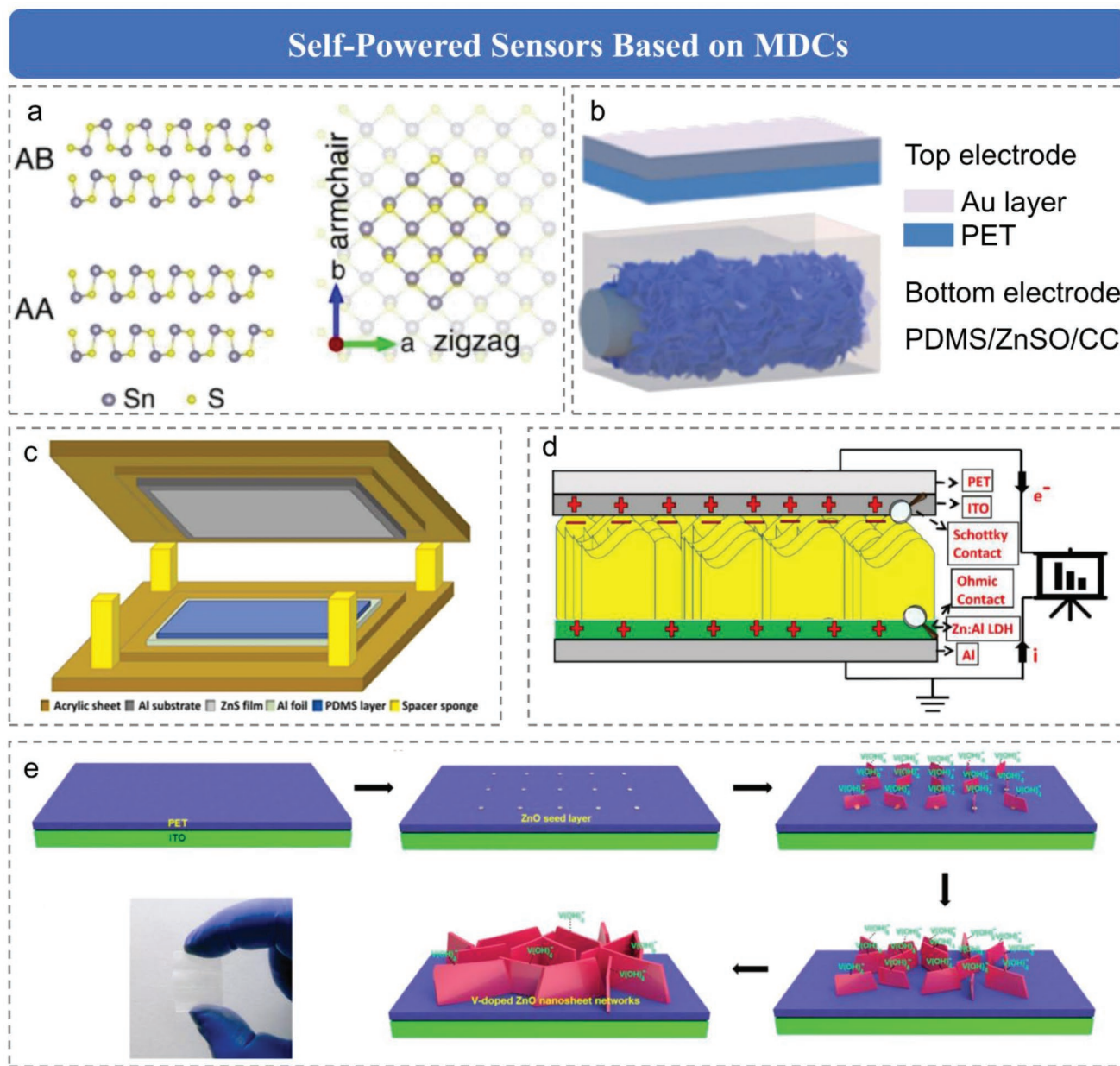
**ADVANCED
SCIENCE NEWS**

www.advancedsciencenews.com

**ADVANCED
FUNCTIONAL
MATERIALS**

www.afm-journal.de

Figure 8. Self-powered NG sensors based on MDCs materials. a) Cross-sectional crystal structures of SnS along the armchair direction with different stacking sequences: non-centrosymmetric AA and centrosymmetric AB staking. Reproduced under terms of the CC-BY license.[207] Copyright 2020, The Authors, published by Springer Nature. b) The schematic illustration structure of the bottom and top electrodes of the FTENG. Reproduced with permission.[121] Copyright 2021, Elsevier Ltd. c) Fabricated TENG schematic. Reproduced with permission.[122] Copyright 2022, Elsevier Ltd. d) Cross-sectional view of the fabricated device. Reproduced with permission.[123] Copyright 2021, Elsevier B.V. e) Schematic diagrams for the growth mechanism of V-doped ZnO. The seed layer was deposited by spin coating on a bare ITO/PET substrate. $V(OH)^{4-}$ ions are connected at the Zn^+ terminated surface, which blocks the 1D growth of V-doped ZnO. Reproduced with permission.[124] Copyright 2013, American Chemical Society.

performance of heterostructures is usually superior to those of devices made from a single material.

The identification of harmful gases in the environment is of great significance to people's lives, which requires sensors with low power consumption, portability, and high sensitivity. Sardana et al. reported a novel MXene/TiO_2/Cellulose-nanofibers (C-NFs) heterojunction gas sensor for NH_3 detection, which is driven by an electrospun TENG. TENG used two biodegradable cellulose films in different electronegativity

as the friction layers (electronegative MXene nanofibers and cellulose acetate nanofibers). The gas sensor exhibited great reproducibility and high selectivity.[128] **Figure 9**a depicts the possible mechanism of MXene/TiO_2/C-NFs heterojunction-based sensor and the electron transfer process between MXene and TiO_2. The electrons of n-type TiO_2 gradually migrate into the conduction band of MXene until the Fermi levels of the two materials flatten. In air, oxygen molecules will capture electrons from the heterojunction surface, which may increase
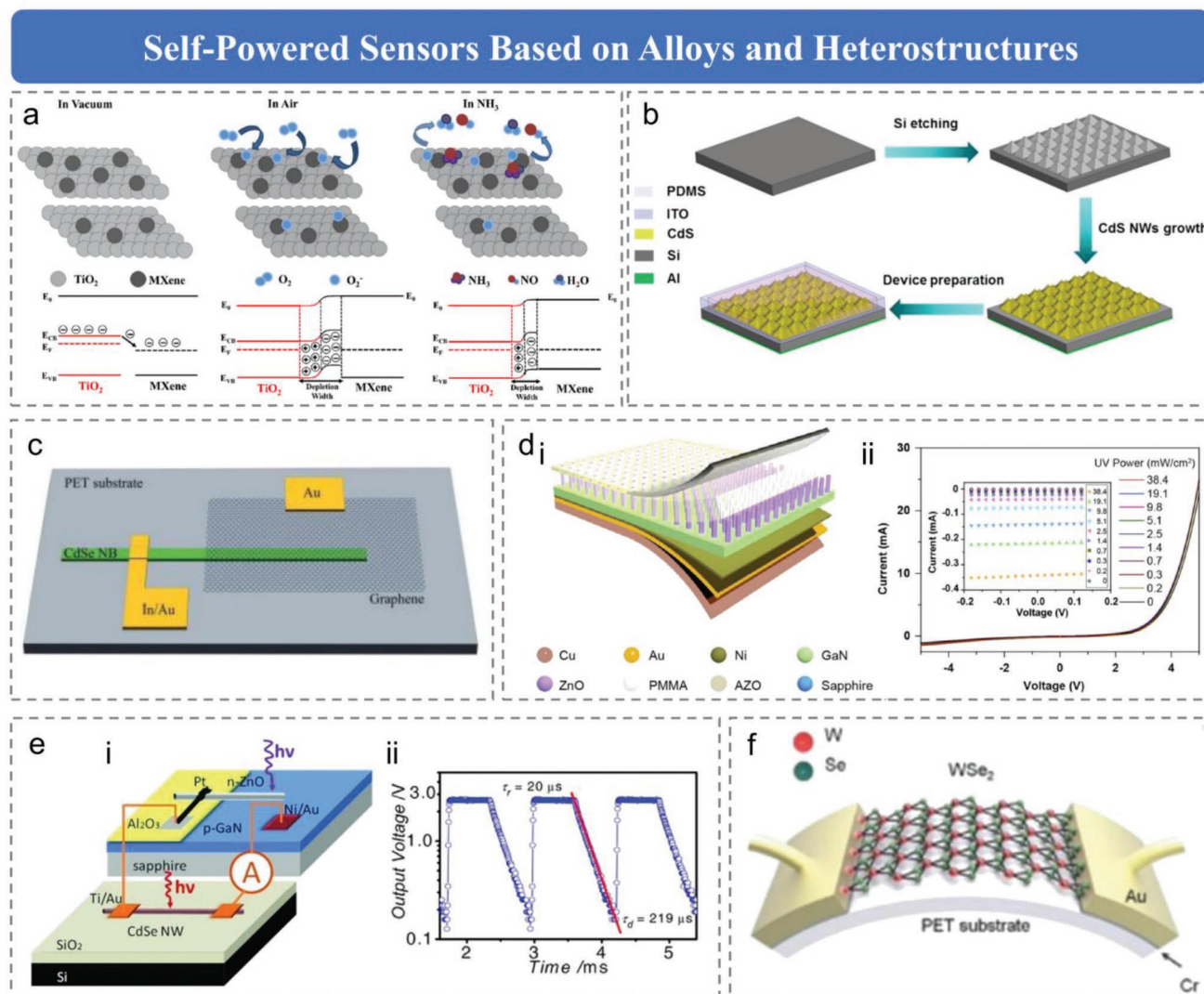
Figure 9. Self-powered NG sensors based on alloys and heterostructures materials. a) Schematic of the gas mechanism of the MXene/TiO$_2$/C-NFs heterojunction-based sensor and electron transfer process between MXene and TiO$_2$. Reproduced with permission.[128] Copyright 2022, American Chemical Society. b) Fabrication process and schematic structure of a Si/n-CdS NWs heterostructure near-infrared photodetector. Reproduced with permission.[131] Copyright 2017, Elsevier Ltd. c) The schematic diagram of the CdSe NB/graphene Schottky junction photovoltaic detector on a PET substrate. Reproduced with permission.[132] Copyright 2013, Royal Society of Chemistry. d) Structural schematic diagram of the p-GaN/n-ZnO hetero-junction-based photodetector and the *I-V* characteristics of GaN/ZnO heterojunction photodetector. Reproduced with permission.[133] Copyright 2022, Elsevier Ltd. e), i) Schematic of the CdSe nanowire device powered by an n-ZnO/p-GaN heterojunction photovoltaic unit. ii) Photoelectrical voltage (logarithmic scale) of the heterojunction as a function of time while the incident UV–light is modulated by a chopper working at 800 Hz. Reproduced with permission.[134] Copyright 2011, Wiley-VCH GmbH. f) Schematic of the piezoelectric energy harvester based on monolayer WSe$_2$. Reproduced with permission.[137] Copyright 2017, Wiley-VCH GmbH.

the width of depletion layer. On the contrary, in the target gas, NH$_3$ molecules interact with pre-adsorbed O^{2-} anions and release the captured electrons back to the heterojunction surface. The conductive channel of MXene reduces the resistance of the heterojunction and accelerates the redox reaction at room temperature, which simultaneously plays an important role in improving the selectivity of the heterojunction.

Since the discovery of graphene in 2004, the variety of 2D materials has been increasing, and the research on 2D materials has been deepening. These novel 2D materials provide new opportunities for the design of high-performance opto-electronic devices, especially in photodetectors.[129,130] Dai et al.

reported a *n*-Si/*n*-CdS heterojunction near-infrared photode-tector, with compression enhanced optical response due to the piezo-phototronic effect,[131] which is the coupling effect of piezoelectric, semiconductor, and light excitation in piezo-electric semiconductors (e.g., CdS with wurtzite structure). Figure 9b shows the fabrication process and structure diagram of Si/CdS heterojunction near-infrared photodetector. This report provides a facile and effective method for enhancing the optical response of 2D-based materials in the near-infrared band by piezo-phototronic effect. Gao et al. reported for the first time a high-performance flexible transparent CdSe nanoribbon/graphene as Schottky junction self-powered photodetector.[132]

**ADVANCED
SCIENCE NEWS**

www.advancedsciencenews.com

**ADVANCED
FUNCTIONAL
MATERIALS**

www.afm-journal.de

As depicted in Figure 9c, the graphene Schottky contact electrode was fabricated on the other end of the CdSe nanoribbon, and a 100 nm-thick Au ohmic contact electrode was fabricated on graphene far away from the CdSe nanoribbon. CdSe/graphene photodetectors show great potential in self-powered, high-sensitivity, fast-tracking, flexible, and transparent optoelectronic applications. Peng et al. reported a self-powered flexible UV–photodetector based on p-GaN/n-ZnO heterostructures.[133] Since both GaN and ZnO are piezoelectric semiconductor materials, the piezoelectric charges generated on both sides of the heterojunction interface under external strain will regulate the separation, extraction, and recombination of photogenerated carriers based on the piezo-phototronic effect. Figure 9di shows the structure of p-GaN/n-ZnO heterojunction-based photodetector. As shown in Figure 9dii, the I–V curves under 325 nm ultraviolet light illumination at different power densities show typical rectification behavior. The photogenerated electron-hole pairs can be effectively separated by the built-in electric field of the p-n heterostructure even when no bias voltage is applied. Therefore, the GaN/ZnO heterostructure photodetector can be used as a self-powered photosensor. Bie et al. reported a device integrating ZnO/GaN heterojunction and CdSe nanowire which could be used for selective multiwavelength photodetectors.[134] CdSe is an important direct transition wide bandgap semiconductor with excellent optical and electrical properties, which is widely used in LEDs. Figure 9e shows the ZnO/GaN heterojunction photodetector device (right) and the change of photoelectric voltage (logarithmic scale) as a function of time. When the incident UV light is modulated by a chopper operating at 800 Hz, the red line is a linear fit of the falling edge of the voltage after the UV light is cut off. The optical response speed of the ZnO/GaN heterojunction is much faster than that of traditional ZnO photodetectors.

Recently, piezoelectricity has been observed in 2D atomically thin materials such as h-BN, graphene, and TMDs.[29,101,135,136] However, due to the insufficient mechanical durability of single-layer TMD materials, it cannot support its continuous operation, so it is not suitable for practical piezoelectric devices. Lee et al. reported the reliable piezoelectric performance of WSe_2 bilayer film.[137] Figure 9f shows the schematic of PENG based on monolayer WSe_2, which consists of W, Se, Cr/Au electrode, and PET substrate. The red and green spheres represent the W and Se atoms, respectively. The WSe_2-based device exhibits strong piezoelectricity and excellent mechanical durability over a large strain range and can harvest enough energy to operate small liquid crystal displays (LCDs) without applying any external bias.

3.6. Self-Powered Sensors with Piezoelectric/Triboelectric Potential Driven Transistors

The emergence of transistors has created the prosperity of electronic products today. Therefore, the transistors have been called the greatest invention of the 20th century, which laid the foundation for the generation of integrated circuits, microprocessors, and computer memory. Nowadays, compared with conventional transistors, triboelectric potential tuned transistors based on TENG have superior output performance but lower

energy.[138–144] At the same time, contact-electrification-controlled transistors have potential applications in various fields, such as neuromorphic computing, memory storage devices, image recognition, and electronic skins.
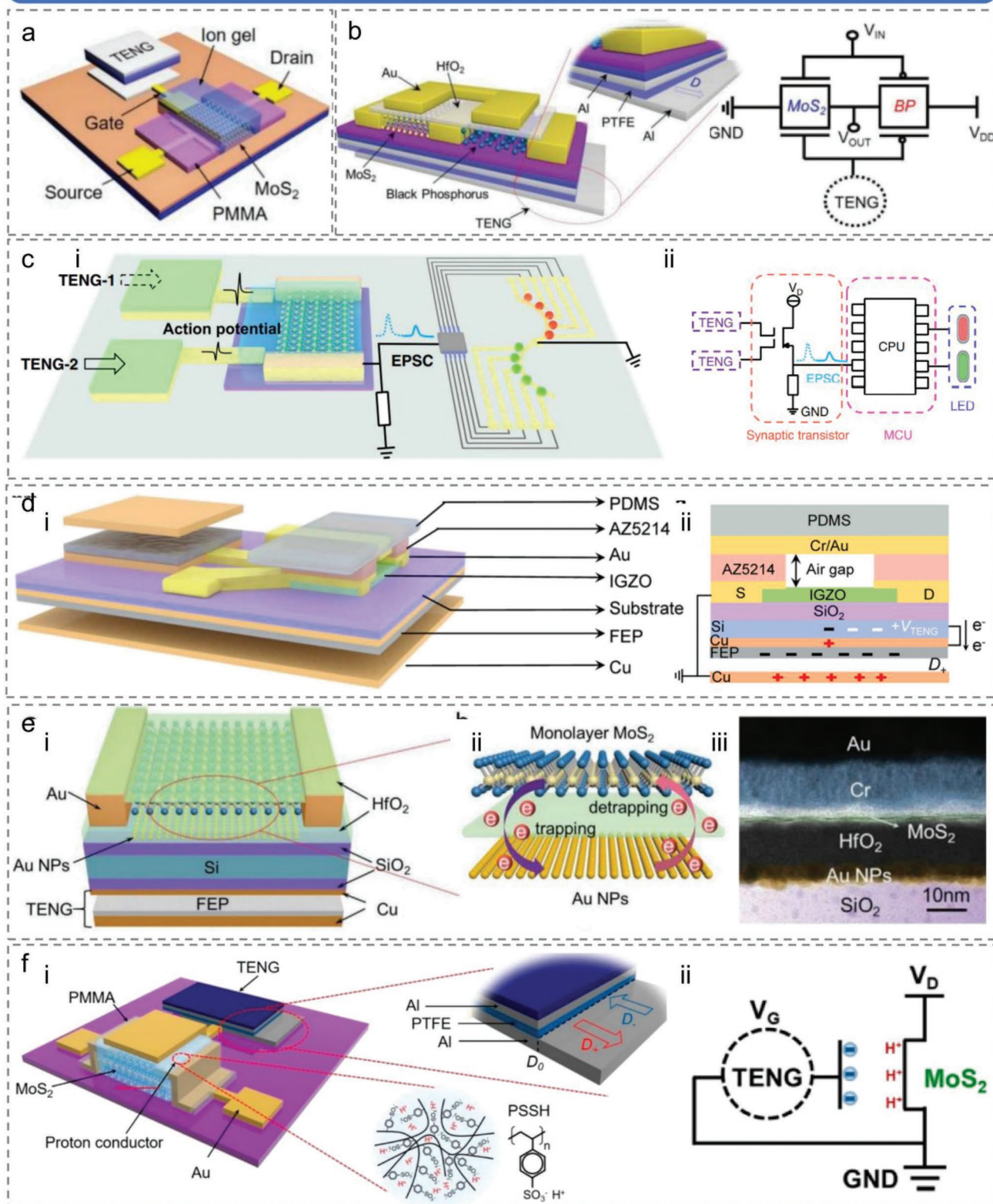
Gao et al. reported for the first time a triboiontronic transistor that combined triboelectric potential modulation with ion-controlled semiconductor devices.[145] As shown in **Figure 10**a, the TENG is composed of a mobile Al friction layer and a fixed PTFE friction layer, and the Al electrode is stuck on the backside. A high-performance triboiontronic MoS_2 transistor with a high current on/off ratio, low threshold, and steep switching characteristics has been developed by using triboelectric potential instead of gate voltage to control the device. This provides a low-power and high-efficiency method for tribo-modulating semiconductor devices, which can provide unprecedented physical properties that interact with mechanical motions. Figure 10b shows the tunable dual-gate tribotronic logic device composed of n-type MoS_2 and p-type BP FETs (left). The triboelectric potential generated by TENG can effectively drive transistors and logic devices, regulating the transport of charge carriers. Furthermore, with the additional top gate structure (right), the displacement of the TENG can tune the electrical properties of FET and inverter, including threshold voltage, inversion point, gain value, and static power dissipation.

Under the contact electrification effect, the induced triboelectric signal activates the ion-gel-gated MoS_2 postsynaptic transistor, which enables the artificial afferent to have the adaptive ability of spatiotemporal recognition/sensation to external stimuli (displacement, pressure, and touch patterns).[146] As shown in Figure 10ci, tribopotential induced by contact electrification activates synaptic transistors and transmits relevant mechanical information to functional terminals. As Figure 10cii depicted, dynamic logic can be reflected in the lighting sequence of LEDs by identifying the different input signals caused by contact electrification. The wide bandgap of 2D MoS_2 can effectively reduce the source-drain driving voltage, improve the transport characteristics of the channel, and achieve low energy dissipation and high-performance neuromorphic signal transmission.

TENGs, which can generate triboelectric potential, can also be easily integrated with dual-gate transistors for a variety of sensing applications. Tan et al. reported a device-level universal sensing platform based on triboelectric potential tuned dual-gate IGZO transistors (with common bottom gates and air dielectric top gates), which can be used as multifunctional sensors (including distance/pressure/optical sensors and photonic artificial synapse).[147] Figure 10d shows the versatile sensing platform based on triboelectric potential tuned dual-gate IGZO transistor. Tribopotential tuned IGZO transistors, which can realize synergistic pressure or optical sensing through mechanical displacement modulation, show potential applications in low-power multifunctional sensors, electronic skin, image recognition, and neuromorphic computing.

Mechanoplastic floating-gate neuromorphic transistors can simulate multiple synaptic behaviors through the synergy of friction-controlled gates and charge trapping, which are of great significance to advanced AI and human-machine interfaces.[143] Figure 10e shows the schematic illustration of the mechanoplastic MoS_2 synaptic transistor and the high-resolution

**ADVANCED
SCIENCE NEWS**

www.advancedsciencenews.com

**ADVANCED
FUNCTIONAL
MATERIALS**

www.afm-journal.de

Self-Powered Sensors with Piezoelectric/Triboelectric Potential Driven Transistors

**ADVANCED
SCIENCE NEWS**

www.advancedsciencenews.com

**ADVANCED
FUNCTIONAL
MATERIALS**

www.afm-journal.de

cross-sectional micrograph of the synaptic transistor by transmission electron microscope. As shown in Figure 10eii, when the triboelectric potential is coupled with MoS_2 channel, the induced carriers are captured by the Au nanoparticle floating gate and gradually decay back through the tunneling layer. This process is used to simulate the neurotransmitter delivery process. Yang et al. reported a multifunctional triboelectric MoS_2 transistor via a complex combination of triboelectric modulation and proton transport.[148] The triboelectric potential is generated by mechanical displacement, and the electrical properties of transistors are tuned by proton migration/accumulation. Figure 10fi shows the triboiontronic transistor via proton conductor, including the enlarged structure of TENG component (top inset) and the chemical structure of poly(styrenesulfonic) acid (PSSH, bottom inset). Figure 10fii depicts an equivalent circuit diagram of the PSSH proton-conductor-gated transistor driven by TENG, which has excellent electrical properties and high current on/off ratio. It provides a theoretical basis for reliable and effective triboelectric potential modulation on electron transport via proton media, promising an important direction of theoretical research in triboelectric gating, active mechanical sensing, self-powered electronic skin, and AI.

4. Applications in Integrated Self-Powered Sensors

Self-powered nanosensor is a new type of sensor developed rapidly in recent years, which is designed by using nanotechnology or nano-effect and can collect and utilize the energy in the environment to achieve continuous work. TENG/PENG self-powered sensors based on 2D materials can collect different forms of mechanical energy in the environment. They have the advantages of wide selection of materials, low production cost, and multi-functional integration, and have broad applications in mobile electronic products, self-driving micro-nano systems, and the new generation of IoT. This part mainly reviews the application of TENG/PENG self-powered sensors based on 2D materials in different fields such as human motion monitoring, energy harvesting, biomedical engineering, environment monitoring, AI, and neuromorphic devices.

4.1. Integrated Sensors for Human Motion Monitoring

Wearable electronic devices have gradually attracted people's attention due to their advantages of convenient portability, small size, and strong flexibility. Self-powered sensors based on various NGs are often used to detect human physical signals.

The application of wearable devices has been expanded with the proposal of electronic skin.[149,150] Recently, wearable electronic devices are often used to monitor human motion and posture. For instance, Wang et al. reported the high-sensitivity TENG self-powered sensors based on graphene woven fabrics (GWFs). The flexible wearable strain sensor was assembled by pasting graphene films on polymer and medical tape composite film.[151] Roy et al. reported the wearable pressure sensor based on GO for detecting human respiration and temperature fluctuations.[152] In the medical field, pulse and respiration are very important factors to reflect and evaluate a person's health, especially for patients with cardiopulmonary diseases. As shown in **Figure 11**a, the piezoresistive sensor based on MXene is installed on the wrist of the human body to detect the pulse beat, because the current pulse is generated with pulse beating. Besides, TENG self-driven sensors based on 2D materials can also be used to detect human motions. Figure 11b depicts a sensor attached to a fingertip that can be used to detect the clapping behavior and generate a corresponding pulse signal. Huang et al. reported the incorporation of 2D MXene into PVDF nanofibers as a positive triboelectric material for TENG sensors via a simple electrospinning technique,[153] as shown in Figure 11ci. The self-powered sensors can effectively detect human walking (Figure 11cii) and arms swinging (Figure 11ciii), which have broad application prospects in wearable electronics. 2D metal-organic frameworks (MOFs) have been widely used due to their tunable pore size, large specific surface area, diverse framework structures, and surface modifiability. MOF-based TENG sensors with large specific surface area and excellent nano-porosity have been reported.[154] The high-performance TENG self-powered sensor in contact-separation mode is shown in Figure 11di, which can be used to detect different motion states of the human body, e.g., walking, slow running, jumping, and falling-down (Figure 11dii). In addition, self-powered sensors based on 2D materials can also enable IoT human motion monitoring. Salauddin et al. reported a smart sensor based on MXene/silicon nanocomposite (Figure 11ei),[155] which not only enables IoT human motion monitoring by smartphone (Figure 11eii) but also realizes anti-theft alarm by sensing human hand touch (Figure 11eiii).

4.2. Integrated Sensors embodying Energy-Harvesting

Mechanical energy in nature is valuable sustainable energy for human beings, which can be converted into electrical energy by NGs.[156] NGs based on 2D materials hold great promise in energy supply due to high power density, low cost, lightness,

---

Figure 10. Self-powered NG sensors with piezoelectric/triboelectric potential-driven transistors. a) Schematic illustration of the triboiontronic transistor of MoS_2. Reproduced with permission.[145] Copyright 2019, Wiley-VCH GmbH. b) Schematic illustration of the tunable dual-gate tribotronic logic device composing of n-type MoS_2 and p-type BP FETs and circuit diagram of the dual-gate tribotronic logic device. Reproduced with permission.[208] Copyright 2018, Wiley-VCH GmbH. c), i) Schematic illustration diagram and ii) a simplified circuit diagram of the artificial afferent for dynamic logic demonstration. Reproduced under terms of the CC-BY license.[146] Copyright 2021, The Authors, published by Springer Nature. d), i) Schematic diagram of the versatile sensory platform based on triboelectric potential tuned dual-gate IGZO transistor and ii) the simplified diagram of the device. Reproduced with permission.[147] Copyright 2021, Elsevier Ltd. e), i) Schematic illustration of the mechanoplastic MoS_2 synaptic transistor, ii) the working mechanism of Au NPs floating-gate layer and iii) high-resolution cross-sectional micrograph of the synaptic transistor by TEM. Reproduced with permission.[143] Copyright 2020, Wiley-VCH GmbH. f), i) Schematic illustration of the triboiontronic transistor via proton conductor and ii) the equivalent circuit diagram of the Poly(styrenesulfonic) acid gated triboiontronic transistor. Reproduced with permission.[148] Copyright 2020, American Chemical Society.
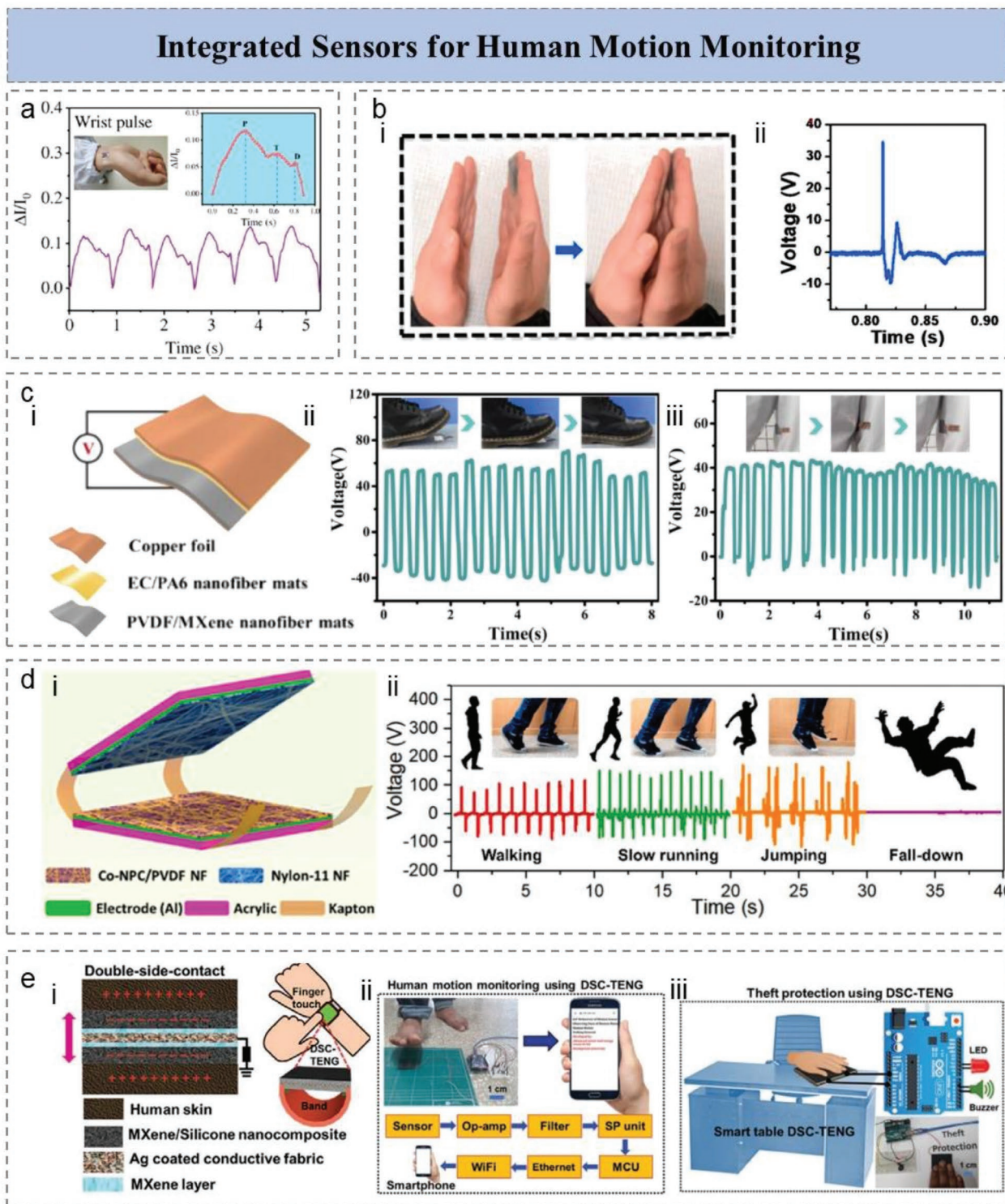
Figure 11. Integrated sensors for human motion monitoring. a) The signal responses in the form of current changes come from wrist pulse (the enlarged illustration is a magnified view of the pulse vibration waveform). Reproduced with permission.[209] Copyright 2020, American Chemical Society. b), i) Peak-to-peak output voltage of the flexible STENG under human body motion: hand clapping. ii) The shape of each generated signal. Reproduced with permission.[210] Copyright 2020, Elsevier Ltd. c), i) Schematic diagrams of the TENG structure. ii) Applications of the all-fiber TENG as a self-powered sensor for human walking and iii) moving of arms. Reproduced with permission.[158] Copyright 2021, American Chemical Society. d), i) Structure design of the MOF-based TENG self-powered sensor. ii) Voltage output under different motion states, i.e., walking, slow running, jumping, and falling down, for the application of a self-powered human motion monitor. Reproduced with permission. [159] Copyright 2022, Elsevier B.V. e), i) Schematic diagram of double-side-contact-based TENG. ii) Photograph of the self-powered human motion monitoring sensor for IoT applications via smartphone and iii) the smart table for data/material theft protection from human skin touch using TENG-based sensor. Reproduced with permission. [160] Copyright 2022, Wiley-VCH GmbH.

**ADVANCED
SCIENCE NEWS**

www.advancedsciencenews.com

**ADVANCED
FUNCTIONAL
MATERIALS**

www.afm-journal.de

and excellent manufacturability.[157] As we all know, human daily activities, such as the movement of different joints and breathing, can generate various mechanical energy. These energies can be efficiently collected through NGs to meet the needs of green energy and sustainable development.[158,159] Kaur et al. reported a single-electrode TENG sensor made of reduced graphene oxide nanoribbons (rGO-NRs) for harvesting mechanical energy from human fingertip strain.[160] **Figure 12**a shows the electromagnetic-triboelectric-hybrid TENG sensor for harvesting human mechanical energy. With 2D MoS_2 as the electron acceptor, it has a very high output response. Song et al. reported a PENG based on 2D PbI_2 nanosheets for converting collected mechanical energy into electrical energy.[136] Figure 12bi shows the growth of several layers of MoS_2 on cellulose paper, followed by in-situ deposition of polarized PVDF nanofibers processed by electrospinning to fabricate a piezoelectric-triboelectric hybrid nanogenerator and to obtain energy from simple manual activities such as handwriting or human touch. When the device feels pressure, it will generate the corresponding pressure signal (Figure 12bii). Kim et al. reported a flexible PENG with directional piezoelectric effect based on monolayer MoS_2 to acquire mechanical stretching energy and enable to double the output.[161] As shown in Figure 12c, graphene was grown on thin copper foil, and the surface negatively charged 2D BP nanosheet particles were exfoliated and deposited on the graphene/Cu electrode. Mechanical energy harvesting can be efficiently performed when the device is under stretching.

With the gradual exhaustion of fossil energy, the utilization of renewable energy (e.g., wind power and hydropower) is one of the most effective ways to solve the global energy crisis.[162–165] The compatibility of NGs also gives them considerable advantages in energy harvesting in the environment. Figure 12d shows a TENG sensor based on 2D ZnO nanowire array that collects heat from the environment and converts it into electricity. Moreover, the self-powered sensor based on GO can also harvest sound energy in the environment, as illustrated in Figure 12e. When the sound is simulated with a tuning fork, the sensor will generate a corresponding current signal. Wind energy has become a potential energy source because of its wide coverage and large amount. Karmakar et al. reported the green chemical preparation of bilayer MoS_2 nanosheets and discovered their applications in triboelectric and catalytic energy harvesting.[166] Figure 12f shows the TENG with excellent tensile properties and sensitivity based on MXene. The wind wave will generate a small pressure on the device, thus causing the vibration of the upper electrode, so that the triboelectric charge is transferred between the upper electrode and the lower electrode. The collected wind energy is converted into electricity, and the electricity can drive color-tunable LEDs.

4.3. Integrated Sensors for Biomedical Engineering

There are highly complex biological signals in the human body, each of which conveys the working state of the body. With the development of information technology in the field of medical research, corresponding sensors can detect different human body information by receiving human body signals to realize

the diagnosis of diseases. Self-powered biomedical sensors based on 2D materials provide a promising power/sensing solution in biomedical applications due to their high sensitivity, simplicity, and portability.[167] Grant et al. reported that GO had broad potential in the biomedical field, which could promote cell proliferation, drug loading, and antibacterial properties of composites with great biocompatibility.[168] MoS_2 and its composites open a new era in nano-sensor fabrication because of exciting catalytic properties and biocompatibility. Sha et al. reported the wide application of self-driven sensors based on MoS_2 in biomedicine.[169] **Figure 13**a shows the structural design of a smart contact lens with an ultrathin MoS_2 transistor serpentine grid sensing system, and the dashed area highlights the gold-mediated mechanical exfoliation of monolayer MoS_2. The device can detect optical signals and corneal temperature, which is essential in ophthalmology-related researches and provides an alternative solution for the manufacture of advanced smart contact lenses.

Implantable medical devices have become an indispensable medical tool to improve the life quality of patients and prolong their life.[170] Self-powered sensors based on 2D materials can also be used for implantable medical detection. As shown in Figure 13b, a flexible and biocompatible pressure sensor based on 2D MXene is applied to the apical epicardium of the mouse chest wall, which can record the vibration of the mouse heart and perform real-time heart beating signal detection. Figure 13c shows a durable, fatigue-resistant soft nerve prosthetic device for bidirectional signal of peripheral nerves. The designed device was implanted into the sciatic nerve of the rat to record sensory nerve signals evoked by mechanical stimulation of the rat foot, providing a solution for clinically challenging neurological diseases.

Wearable non-invasive glucose sensors provide humans with a painless and portable means of blood glucose monitoring and health management and have attracted much attention in recent years.[171] Figure 13d shows the schematic diagram of a non-invasive blood glucose sensor, using two textile-like graphene-based electrodes attached to the back of the hand and wrist. The blood glucose level of the test subject changed before and after breakfast, lunch, and the dual-electrode non-invasive glucose sensor could well monitor this change. In addition, Yang et al. reported that the self-driven sensor based on LIG can be applied to human electrocardiogram (ECG) monitoring. As shown in Figure 13e, the 12-lead ECG consists of 4 extremity electrodes and 6 thoracic electrodes. The thoracic lead ECG signal is shown in Figure 13eii. The ECG obtained by the test is consistent with that of healthy people.

4.4. Integrated Sensors for Environment Monitoring

With the attention to environmental quality, in the actual environmental detection process, people often need analytical equipment and instruments that can be easily carried and can continuously and dynamically monitor a variety of analytes. Current environmental monitoring sensors usually require external energy, such as batteries. For long-time working sensors, the battery not only has limited life but also brings environmental pollution problems.[172–175] TENG/PENG self-powered sensors
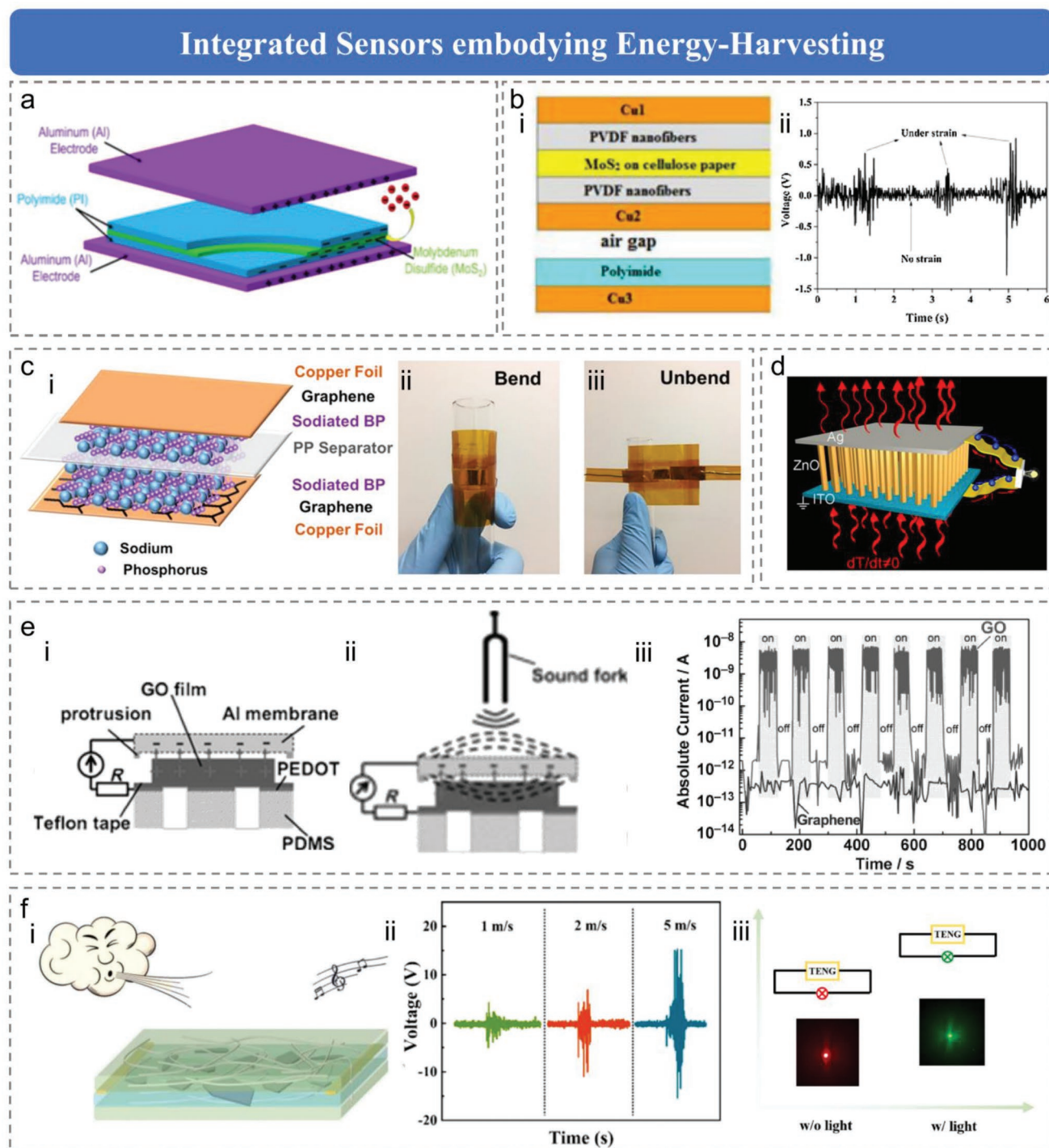
**ADVANCED
SCIENCE NEWS**
www.advancedsciencenews.com

**ADVANCED
FUNCTIONAL
MATERIALS**
www.afm-journal.de

Figure 12. Integrated sensors embodying energy harvesting. a) Illustration of the vertical contact-separation mode TENG with a MoS$_2$ layer. Reproduced with permission.[211] Copyright 2020, Elsevier Ltd. b), i) Structure of the hybrid nanogenerator. ii) Graphs showing the open circuit voltage of pristine MoS$_2$ grown on cellulose paper. Reproduced with permission.[212] Copyright 2018, Elsevier Ltd. c), i) Schematic representation of the configuration of the BP mechanical energy harvester. Representative images of ii) bending and iii) unbending performed on the developed energy harvester. Reproduced with permission.[213] Copyright 2017, American Chemical Society. d) Schematic diagram showing the structure of the pyroelectric nanogenerator. Reproduced with permission.[214] Copyright 2012, American Chemical Society. e), i) Schematic of the device. ii) Schematic of applying sound fork to the device. iii) Current of GO/graphene nanogenerator versus sound fork vibration. Reproduced with permission.[215] Copyright 2012, Wiley-VCH GmbH. f), i) The structure of multifunctional TENG to detect small wave vibration. ii) Voc of TENG with different wind speeds. iii) Alterable colored LED shows different light at different environment. Reproduced with permission.[216] Copyright 2021, Elsevier Ltd.

**ADVANCED
SCIENCE NEWS**

www.advancedsciencenews.com

**ADVANCED
FUNCTIONAL
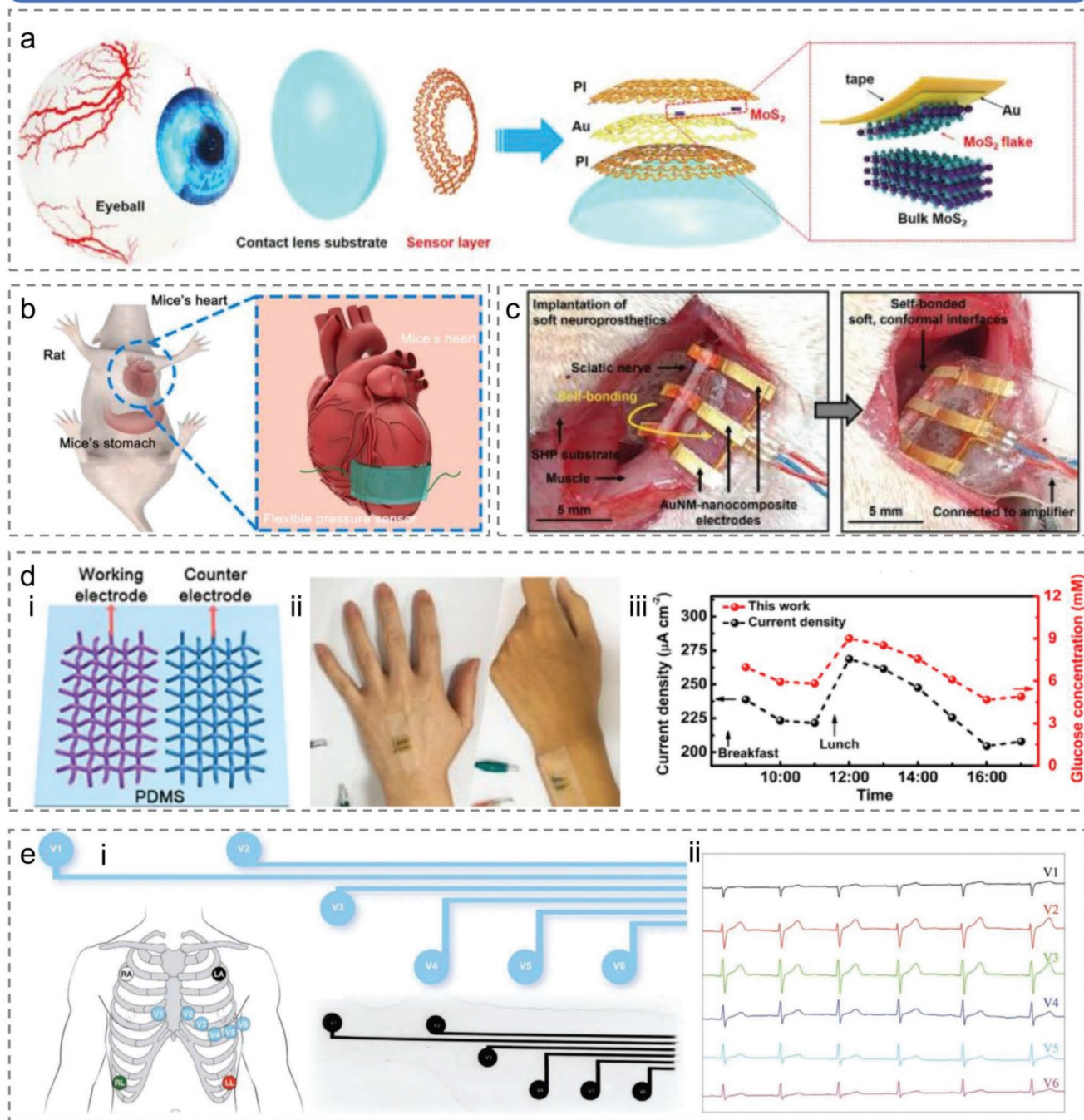MATERIALS**

www.afm-journal.de

Figure 13. Integrated sensors for biomedical engineering. a) Schematic illustration of the different layers of smart contact lens structure attached to an eyeball. The dashed region highlights the gold-mediated mechanical exfoliation of monolayer MoS₂. Reproduced with permission. [217] Copyright 2020, Elsevier Inc. b) Schematic of the pressure sensor attached to the heart of mice. Reproduced with permission. [218] Copyright 2021, Elsevier Ltd. c) Photographs showing the implantation of fatigue-resistant soft neuroprosthetics. Reproduced with permission.[219] Copyright 2021, Wiley-VCH GmbH. d), i) Schematic of the non-invasive blood glucose sensor by using two textile-like electrodes. ii) Digital photographs of non-invasive blood glucose sensors attached on the hand back and wrist of healthy volunteers. iii) The blood glucose monitoring conducted by the non-invasive glucose sensors on two healthy volunteers for 8 h. Reproduced with permission [220] Copyright 2021, Elsevier B.V. e), i) Positions of 12-lead ECG electrodes. ii) 12-lead ECG signals (5 s) recorded by LIG/PDMS electrodes: chest leads. Reproduced with permission.[22] Copyright 2021, Wiley-VCH GmbH.

ADVANCED
SCIENCE NEWS
www.advancedsciencenews.com

ADVANCED
FUNCTIONAL
MATERIALS
www.afm-journal.de

show continuous good performance to the environment, and the excellent properties of 2D materials make NGs widely used in environmental monitoring. **Figure 14**a shows a high-performance flexible SnS_2/rGO nanohybrid humidity sensor driven by PTFE-based TENG. Taking the output voltage and relative humidity of the friction humidity sensor as a function, the regression coefficient is 0.998, and the fitting result is great.

There are many gases in the environment. When the human body inhales a large amount of certain gases, it will cause immeasurable harm to the body. Therefore, it is very necessary to realize gas detection in the environment. As shown in Figure 14b, the resistance of TENG-driven sensor based on PANI/MXene composite for detecting NH_3 in the environment increases with increasing NH_3 concentration. The resistance of PANI sensor is ≈40 kΩ in air and exceeds 50 kΩ in 10 ppm NH_3, the resistance of PANI/MXene composite sensor is ≈22 kΩ in air and over 30 kΩ in 10 ppm NH_3 environment. Compared to pure PANI sensor, the doping of MXene reduces the resistance of the sensor and increases the response value of the sensor. The PANI/MXene composite sensor also shows better sensitivity at different NH_3 concentrations (Figure 14bii). The dependence of the sensor response on humidity and NH_3 concentration can be fitted linearly, as shown in Figure 14biii. The novel flexible self-powered sensor based on PENG with 2D $MoSe_2$ flakes can also efficiently detect NH_3 in the environment (Figure 14c). The output voltages of $MoSe_2$-based sensors when exposed to different concentrations of NH_3 are quite different. Moreover, Lee et al. reported an ultra-high-sensitivity gas sensor based on 2D MXene capable of detecting polar and non-polar chemicals in the environment, including hydrogen and methane with very low detection limits of 2 and 25 ppm, respectively.[176] Ou et al. reported a self-powered sensor based on SnS_2 flakes with physical affinity to NO_2, providing a real solution for low-cost and selective NO_2 gas sensing.[177] More and more attention has been paid to the potential applications of heterojunction synthesis in catalysis and gas sensors. Qiao et al. creatively reported a sensor based on MoS_2/SnO_2 *p-n* heterojunction for detecting trimethylamine in the environment, which had the advantages of high sensitivity, high selectivity, high stability, and high catalytic activity.[178] In addition to the nanosensors driven by NGs, NGs themselves can also act as self-powered sensors based on novel active materials or sophisticated structures. As shown in Figure 14d, the PENG sensor based on SnO_2/ZnO nanoarray realizes high H_2 detection at room temperature. Since the SnO_2 nanoparticles loaded on the surface of ZnO NWs can act as a catalyst for the H_2 oxidation reaction, the PENG itself can be used as a gas sensor. When the sensor is exposed to the H_2 environment, H_2 undergoes an oxidation reaction, and the electrons released by the oxidation reaction flow back to the conduction band of the ZnO NWs. The sensitivity of the sensor under different H_2 concentrations is different, and the sensitivity increases with the increment of H_2 concentration.

4.5. Integrated Sensors for Artificial Intelligence and Neuromorphic Devices

With the development of AI, more and more sensors are being researched and developed.[179–181] The ideal smart sensor should

have the characteristics of light-weight, flexibility, comfort, and long service life. There are still many difficulties in existing sensor devices due to the energy storage limitation of batteries, so TENG/PENG solves these difficulties well with its excellent characteristics. Robot-like, human-machine interfaces, neuromorphic devices, etc. are all hotspots in AI research today. The self-powered devices and systems based on 2D materials perfectly combine the advantages and make great progress in the field of AI.

The NG self-powered device based on 2D materials is shown in **Figure 15**. Figure 15a depicts mechanoluminescent hybrid-material sensors based on 2D ZnS, which enable humanoid robots to sense external stimuli while exchanging information with humans. The wireless sensing system can be used for remote information interaction and health monitoring. The user interface with sensory feedback is very important, so that the interaction information between humanoid robots and humans can be reflected in the application program interface. This work inspires people to explore and expand the applications of multimodal sensors based on 2D materials, in the field of AI.[182–184] As shown in Figure 15b, based on the interaction between human and 3D printing manipulator, an intelligent human-machine interface is established. SnS_2 nanomaterials are integrated into a PENG device to explore the human-machine simultaneous control of an intelligent sign language system. The SnS_2-PENG device attached to the human index finger synchronously generates corresponding activation voltages with the different bending states of the index finger to drive the robot index finger. This not only pushes the development of devices based on 2D materials toward multifunctional bio-piezoelectricity but also opens a path to developing human-machine interfaces in near future.[185,186] Figure 15c shows the integration of a single-layer graphene transparent tactile sensor on the bionic finger bone and the use of tactile feedback to control the grasping of soft objects. The sensor placed on the phalanx received a maximum $\Delta V/V_0$ of 115%, and when the $\Delta V/V_0$ exceeded a threshold (115%), the grasping motion of each finger ceased. By imitating human grasping characteristics, the grasping of robot fingers is more accurate.

In recent years, various large-area growth methods for 2D TMDs have been developed for future electronic and photonic applications. However, they have not yet been used for synthetic image sensors. The image sensing properties of a bilayer MoS_2 active pixel image sensor array are successfully investigated using the optical template projection technique, as shown in Figure 15d. Turtle templates (24 × 24 pixels in total) were prepared using a laser cutting system and patterned (Figure 15di). During the light projection, the templates divided into 9 blocks (Figure 15dii) are sequentially placed on the active pixel image sensor array (Figure 15diii). The photosensitive mapping results of the active pixel image sensor array were obtained by light template projection, indicating the successful perception of turtle images (Figure 15div,v).

Sun et al. reported a piezoelectric programmable non-volatile memory integrating PENG and IGZO field effect transistors.[187] Memory storage devices have potential application in low-power wearable health monitoring systems based on human-computer interaction. With the help of biomechanics and vision, the perceptual and cognitive abilities of the human
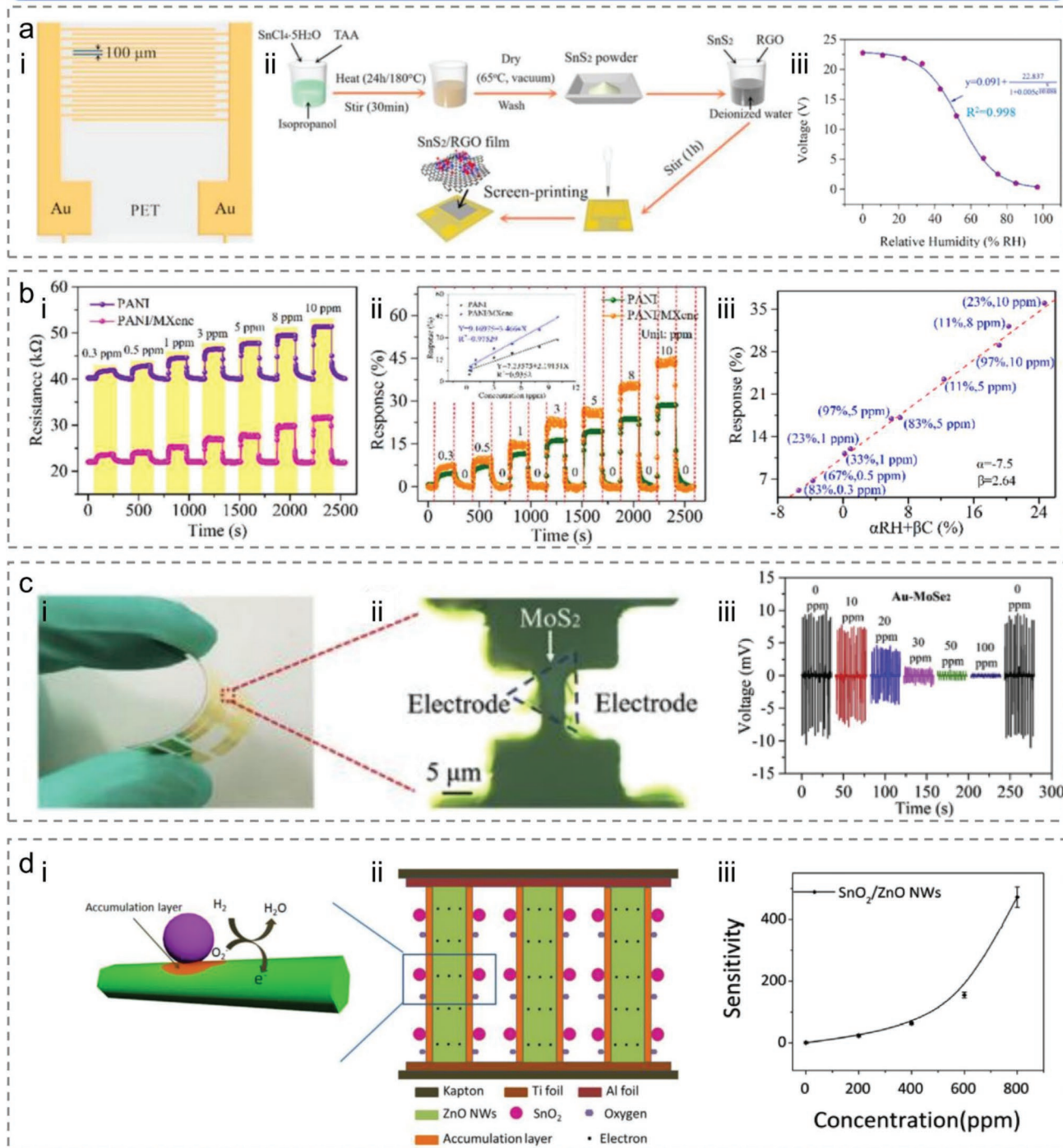
Figure 14. Integrated sensors for environment monitoring. a), i) Schematic of the device ii) Fabrication of the SnS₂/RGO film sensor. iii) The output voltage of the TEHS as a function of relative humidity. Reproduced with permission.[222] Copyright 2019, Elsevier Ltd. b), i) The resistance changes of PANI/MXene hybrid sensor and PANI single sensor under different NH₃ concentrations at 20 °C, ii) resistance response of PANI/MXene and PANI under different NH₃ concentrations at 20 °C and response as a function of PANI/MXene and PANI under different NH₃ concentrations at 20 °C. iii) Linear behavior of the response vs. both humidity and NH₃ concentration for PANI/MXene film sensor. Reproduced with permission.[223] Copyright 2021, Elsevier Ltd. c), i) Photograph of the flexible PENG device. ii) Optical microscope image of a MoS₂ piezoelectric device with two electrodes. iii) MoSe₂ composite-based PEAS upon exposure to different concentrations of NH₃. Reproduced with permission.[224] Copyright 2019, Elsevier Ltd. d), i,ii) SnO₂/ZnO heterostructure in H₂ without applied force. iii) The sensitivity of SnO₂/ZnO NW arrays upon exposure to different concentrations of H₂. Reproduced with permission.[225] Copyright 2014, Elsevier Ltd.
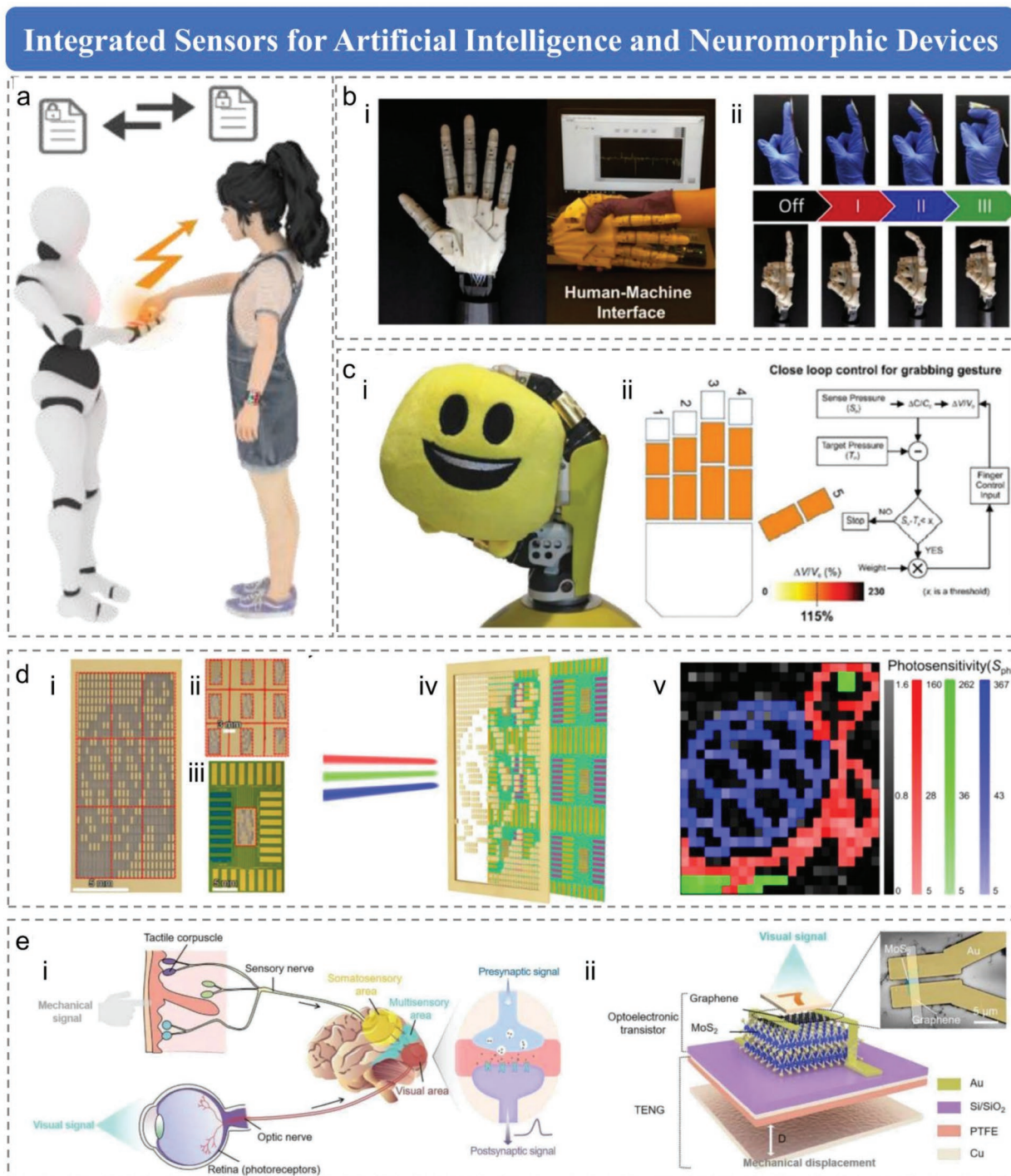
Figure 15. Integrated sensors for artificial intelligence and neuromorphic devices. a) Concept of the bimodal sensor as user-interactive interface of robotics for the perception of external stimuli of temperature and pressure and simultaneously the conversion of pressure into encrypted information that can be recognized by robotics and visible to humans. Reproduced with permission.[226] Copyright 2022, American Chemical Society. b), i) An intelligent human-robotic interface is established based on the interaction between human and 3D printing robotic hands. ii) The snapshot photos of a human forefinger in different bending states (from the off, I, II, to III states). Reproduced with permission.[227] Copyright 2020, Elsevier Ltd. c), i) Grabbing of a softball enabling tactile feedback. ii) Color map of the capacitive sensors, showing the readout voltage modulation after grabbing with tactile feedback enable. Reproduced with permission.[228] Copyright 2017, Wiley-VCH GmbH. d), i) Photograph of the designed turtle stencil. ii) Separated turtle stencils for individual light stencil projection on sensor array. iii) Top view of the image sensor array. iv) Measurement concept using the light stencil projection for image detection of the image sensor array. v) Photosensitivity mapping result extracted from image detection of bilayer MoS_2 image sensor array. Reproduced under terms of the CC-BY license.[229] Copyright 2021, The Authors, published by Springer Nature. e), i) Schematic illustrations of biological tactile/visual sensory system. ii) Schematic diagram of the mechano-photonic artificial synapse based on graphene/MoS_2 heterostructure. Reproduced with permission.[230] Copyright 2021, American Association for the Advancement of Science.

brain are the key to obtaining somatosensory and visual information (Figure 15ei). Inspired by the brain and nervous system, the mechanophotonic artificial synapse device based on graphene/MoS_2 heterostructure is shown in Figure 15eii. The cyan regions are MoS_2 flakes, and the white strips are graphene. It consists of a phototransistor based on graphene/MoS_2 heterostructure and an integrated TENG. Self-powered triboelectric potential-gated transistors have propelled their development and applications in the field of neuromorphic devices.

5. Conclusions and Perspectives

This review focuses on the excellent piezoelectric and optoelectronic properties, triboelectric series of 2D materials, and the self-powered sensors based on various 2D materials and their applications are also introduced. Since the discovery of the first 2D material (graphene), the research of 2D materials has become a popular direction. Some other 2D materials were subsequently prepared, such as graphene-like materials (MXene, h-BN, etc.), TMDs (MoS_2, WS_2, WSe_2, etc.), MDCs (SnSe, GeS, SnS, GaSe, GaS, etc.), alloys and heterostructures, etc. Since the discovery of the piezoelectric properties of MoS_2, the concept of piezotronics, and piezo-photontronics was first introduced to the 2D field. A decisive condition for piezoelectric materials is that their structure has an asymmetric center. For 2D materials without piezoelectricity, such as graphene, piezoelectricity can be achieved by artificially introducing asymmetric centers into the crystal structure or by surface modification engineering and structural control processes. The variation of optical properties of 2D materials with the number of layers can be characterized by the following methods, such as optical contrast spectroscopy, Rayleigh scattering, Raman spectroscopy, optical absorption spectroscopy, and photoluminescence spectroscopy. As the number of 2D materials layers increases, the peaks, intensity, linewidths, or line types of these spectra may change significantly, or some new optical features may appear. In the reported work, large-area graphene films, 2D ZnO, Gr, Si, Gr/ZnO, Gr/Si, and ZnO/Gr/Si heterostructures have excellent optical properties.[152,188–193] At the same time, TMDs have excellent optoelectronic properties due to their semiconducting properties and high absorption coefficients in the spectral range.

As a new energy technology, NG breaks the limitation of traditional energy devices and equipment relying on batteries, which are not only environmentally friendly but also highly recyclable.[163,194–200] However, due to the large internal resistance of TENG and special materials requirement for PENG, the output current is small, and the total output power of the device is limited. Therefore, the integration of TENG/PENG and 2D materials can effectively improve the output power and energy conversion efficiency. The NG self-powered sensors based on different kinds of 2D materials have been applied in many fields such as human motion sensing, energy harvesting, biomedicine engineering, environmental monitoring, AI, and neuromorphic computing. It is foreseeable that the further development of this technology will bring greater significance, it will not only improve the performance of the sensor but also better serve the activities in our daily life. In future research,

the further development of self-powered TENG/PENG sensors based on 2D materials needs to consider the following aspects:

1. Energy Conversion Efficiency: Another application of nano-energy is a self-driven sensing system, which solves the micro-power problem that restricts the development of the IoT, thereby realizing the stability and reliability of wireless sensors under unattended conditions. Therefore, high energy conversion efficiency and output performance are very important in the working process of NGs. We propose that better integration of 2D materials with NGs can be considered to achieve the overall output performance of the device. For example, for 2D graphene, increasing the number of layers in the graphene structure can improve its work function, thus improving the energy conversion efficiency of NG sensors based on graphene. Introducing 2D MXene nanosheets for dielectric modulation can improve the permittivity and surface charge density of NG sensors based on MXene.

2. Suitable Materials: Different 2D materials have distinct electronic band structures, optical, and electrical properties. In particular, the structure matching and function complementary 2D heterojunction materials play a very important role in the fabrication of self-powered TENG/PENG sensors. Selecting suitable materials from numerous 2D materials by means of calculation and simulation is a key problem in the research of self-powered sensors.

3. Process Optimization and Device Structure Design: The structure design of the device determines its output performance in principle. In addition, the preparation of the device is a complex process, it will be in contact with different substances in different environments, and each link will affect the final detection performance of the device, thus the device process optimization is the guarantee of its good performance. Researchers can optimize the corresponding device structure in the context of specific applications using the appropriate process. For instance, the fabrication of 2D ZnS nanostructures using a simple low-temperature hydrothermal synthesis method is helpful for large-scale production.

In summary, the research on NG self-powered sensors based on 2D materials is still in the initial stage, and the selection of 2D materials, device optimization, structure design, stability, and other aspects are still worthy of consideration. However, challenges and opportunities coexist. With the continuous discovery of new 2D materials, NG self-powered active sensors based on 2D materials will also be better applied in human monitoring, energy harvesting, biomedicine, and AI.

Acknowledgements

**ADVANCED
SCIENCE NEWS**

www.advancedsciencenews.com

**ADVANCED
FUNCTIONAL
MATERIALS**

www.afm-journal.de

Conflict of Interest

The authors declare no conflict of interest.

Keywords

[1] N. Armaroli, V. Balzani, *Angew. Chem., Int. Ed.* **2007**, *46*, 52.

[2] R. Dutta, *Encyc. Renew. Sustain. Mater.* **2020**, *3*, 821.

[3] J. Zeng, L. Bi, Y. Cheng, B. Xu, A. K.-Y. Jen, *Nano Res. Energy.* **2022**, *1*, e9120004.

[4] Z. L. Wang, *Mater. Today.* **2017**, *20*, 74.

[5] S. Niu, Z. L. Wang, *Nano Energy.* **2015**, *14*, 161.

[6] J. Li, C. Wu, I. Dharmasena, X. Ni, Z. Wang, H. Shen, S.-L. Huang, W. Ding, *Intell. Converg. Networks* **2020**, *1*, 115.

[7] X. Cao, Y. Xiong, J. Sun, X. Zhu, Q. Sun, Z. L. Wang, *Adv. Funct. Mater.* **2021**, *31*, 33.

[8] Z. Liu, Z. Zhao, X. Zeng, X. Fu, Y. Hu, *Nano Energy.* **2019**, *59*, 295.

[9] X. Ding, H. Cao, X. Zhang, M. Li, Y. Liu, *Sensors.* **2018**, *18*, 1713.

[10] M. Zhu, Q. Shi, T. He, Z. Yi, Y. Ma, B. Yang, T. Chen, C. Lee, *ACS Nano.* **2019**, *13*, 1940.

[11] S. A. Han, J. H. Lee, W. Seung, J. Lee, S. W. Kim, J. H. Kim, *Small.* **2021**, *17*, 3519.

[12] P. Lin, C. Pan, Z. L. Wang, *Mater. Tod. Nano.* **2018**, *4*, 17.

[13] L. Xu, T. Jiang, P. Lin, J. J. Shao, C. He, W. Zhong, X. Y. Chen, Z. L. Wang, *ACS Nano.* **2018**, *12*, 1849.

[14] J. Safaei, G. Wang, *Nano Res. Energy.* **2022**, *1*, e9120008.

[15] X. Liu, T. Ma, N. Pinna, J. Zhang, *Adv. Funct. Mater.* **2017**, *27*, 1702168.

[16] E. Singh, P. Singh, K. S. Kim, G. Y. Yeom, H. S. Nalwa, *ACS Appl. Mater. Interfaces.* **2019**, *11*, 11061.

[17] T. Cai, X. Liu, J. Ju, H. Lin, H. Ruan, X. Xu, S. Lu, Y. Li, *Mater. Lett.* **2022**, *306*, 130904.

[18] D. Wang, D. Zhang, J. Guo, Y. Hu, Y. Yang, T. Sun, H. Zhang, X. Liu, *Nano Energy.* **2021**, *89*, 106410.

[19] J. Dong, J. Liu, L. Tan, C. Xu, J. Zhang, Z. Qiao, D. Chu, Y. Liu, Q. Zhang, J. Jiang, Y. Han, A. P. Davis, Y. Cui, *Nature.* **2022**, *602*, 606.

[20] Z. Liu, A. Dibaji, D. Li, S. Mateti, J. Liu, F. Yan, C. J. Barrow, Y. Chen, K. Ariga, W. Yang, *Mater. Tod.* **2021**, *44*, 194.

[21] K. Xu, K. Wang, W. Zhao, W. Bao, E. Liu, Y. Ren, M. Wang, Y. Fu, J. Zeng, Z. Li, W. Zhou, F. Song, X. Wang, Y. Shi, X. Wan, M. S. Fuhrer, B. Wang, Z. Qiao, F. Miao, D. Xing, *Nat. Commun.* **2015**, *6*, 8119.

[22] G. Liang, X. Li, Y. Wang, S. Yang, Z. Huang, Q. Yang, D. Wang, B. Dong, M. Zhu, C. Zhi, *Nano Research Energy* **2022**, *1*, e9120002.

[23] R. T. Paine, C. K. Narula, *Chem. Rev.* **1990**, *90*, 73.

[24] X. Jiang, S. Liu, W. Liang, S. Luo, Z. He, Y. Ge, H. Wang, R. Cao, F. Zhang, Q. Wen, J. Li, Q. Bao, D. Fan, H. Zhang, *Laser Photonics Rev.* **2018**, *12*, 229.

[25] M. Naguib, M. Kurtoglu, V. Presser, J. Lu, J. Niu, M. Heon, L. Hultman, Y. Gogotsi, M. W. Barsoum, *Adv. Mater.* **2011**, *23*, 4248.

[26] D. Tan, C. Jiang, N. Sun, J. Huang, Z. Zhang, Q. Zhang, J. Bu, S. Bi, Q. Guo, J. Song, *Nano Energy.* **2021**, *90*, 229.

[27] W. Wu, L. Wang, Y. Li, F. Zhang, L. Lin, S. Niu, D. Chenet, X. Zhang, Y. Hao, T. F. Heinz, J. Hone, Z. L. Wang, *Nature.* **2014**, *514*, 470.

[28] S. A. Han, T. H. Kim, S. K. Kim, K. H. Lee, H. J. Park, J. H. Lee, S. W. Kim, *Adv. Mater.* **2018**, *30*, 1800342.

[29] H. Zhu, Y. Wang, J. Xiao, M. Liu, S. Xiong, Z. J. Wong, Z. Ye, Y. Ye, X. Yin, X. Zhang, *Nat. Nanotechnol.* **2015**, *10*, 151.

[30] W. Li, J. Li, *Nano Res.* **2015**, *8*, 3796.

[31] K. Chang, F. Küster, B. J. Miller, J.-R. Ji, J.-L. Zhang, P. Sessi, S. Barraza-Lopez, S. S. P. Parkin, *Nano Lett.* **2020**, *20*, 6590.

[32] M. Buscema, D. J. Groenendijk, G. A. Steele, H. S. van der Zant, A. Castellanos-Gomez, *Nat. Commun.* **2014**, *5*, 4651.

[33] S. Yang, C. Wang, C. Ataca, Y. Li, H. Chen, H. Cai, A. Suslu, J. C. Grossman, C. Jiang, Q. Liu, S. Tongay, *ACS Appl. Mater. Interfaces* **2016**, *8*, 2533.

[34] M. Dai, H. Chen, R. Feng, W. Feng, Y. Hu, H. Yang, G. Liu, X. Chen, J. Zhang, C. Y. Xu, P. Hu, *ACS Nano.* **2018**, *12*, 8739.

[35] M. Fontana, T. Deppe, A. K. Boyd, M. Rinzan, A. Y. Liu, M. Paranjape, P. Barbara, *Sci. Rep.* **2015**, *5*, 12589.

[36] L. Meng, L. Li, *Nano Research Energy.* **2022**, *1*, 9120020.

[37] J. Wang, J. Song, X. Mu, M. Sun, *Mater. Tod. Phys.* **2020**, *13*, 100196.

[38] C. Casiraghi, A. Hartschuh, E. Lidorikis, H. Qian, H. Harutyunyan, T. Gokus, KS. Novoselov, AC. Ferrari, *Nano Lett.* **2007**, *7*, 2711.

[39] Z. Sun, H. Chang, *ACS Nano.* **2014**, *8*, 4133.

[40] Y. Lei, C. Fang, J. Xu, Y. He, *Ceram. Int.* **2016**, *42*, 5326.

[41] Y. Lei, Y. Wang, P. Du, Y. Wu, C. Li, B. Du, L. Luo, Z. Sun, B. Zou, *Mater. Sci. Semicond. Process.* **2022**, *141*, 106416.

[42] M. Xu, T. Liang, M. Shi, H. Chen, *Chem. Rev.* **2013**, *113*, 3766.

[43] A. M. Satawara, G. A. Shaikh, S. K. Gupta, P. N. Gajjar, *Mater. Tod. Proceedings.* **2021**, *47*, 529.

[44] T. S. Zhuravleva, E. P. Krinichnaya, O. P. Ivanova, I. V. Klimenko, A. S. Golub, N. D. Lenenko, I. A. Misurkin, S. V. Titov, *Thin Solid Films.* **2012**, *520*, 3125.

[45] N. N. Hieu, V. V. Ilyasov, T. V. Vu, N. A. Poklonski, H. V. Phuc, L. T. T. Phuong, B. D. Hoi, C. V. Nguyen, *Superlattices Microstruct.* **2018**, *115*, 10.

[46] J. Ge, Y. Zhang, H. Dong, L. Zhang, *Appl. Surface Sci.* **2022**, *574*, 151594.

[47] C. Cong, J. Shang, Y. Wang, T. Yu, *Adv. Optical Mater.* **2018**, *6*, 1700767.

[48] H. Li, J. Wu, Z. Yin, H. Zhang, *Acc. Chem. Res.* **2014**, *47*, 1067.

[49] D. Gupta, R. Kumar, *Radiat. Phys. Chem.* **2022**, *197*, 110144.

[50] S. Roy, P. Bermel, *Sol. Energy Mater. Sol. Cells.* **2018**, *174*, 370.

[51] Y.-H. Zhang, M.-L. Zhang, Y.-C. Zhou, J.-H. Zhao, S.-M. Fang, F. Li, *J. Mater. Chem. A.* **2014**, *2*, 13129.

[52] Z. Liu, H. Yang, J. Wang, T. Li, Y. Hu, P. Yang, *Ceram. Int.* **2021**, *47*, 28985.

[53] S. Garain, S. Jana, T. K. Sinha, D. Mandal, *ACS Appl. Mater. Interfaces.* **2016**, *8*, 4532.

[54] J. Wang, H. Yang, P. Yang, *Composites, Part B.* **2022**, *233*, 109645.

[55] C. Huang, S. Wu, A M. Sanchez, JJP. Peters, R. Beanland, JS. Ross, P. Rivera, W. Yao, DH. Cobde, X. Xu, *Nat. Mater.* **2014**, *13*, 1096.

[56] S. A. Han, J. Lee, J. Lin, S.-W. Kim, J. H. Kim, *Nano Energy.* **2019**, *57*, 680.

[57] Y. Liu, J. Ping, Y. Ying, *Adv. Funct. Mater.* **2021**, *31*, 2009994.

[58] S. Pan, Z. Zhang, *Friction.* **2018**, *7*, 2.

[59] H. Zou, Y. Zhang, L. Guo, P. Wang, X. He, G. Dai, H. Zheng, C. Chen, A. C. Wang, C. Xu, Z. L. Wang, *Nat. Commun.* **2019**, *10*, 1427.

[60] S. Kim, M. K. Gupta, K. Y. Lee, A. Sohn, T. Y. Kim, K.-S. Shin, D. Kim, S. K. Kim, K. H. Lee, H.-J. Shin, D.-W. Kim, S.-W. Kim, *Adv. Mater.* **2014**, *26*, 3918.

[61] J. C. Spear, B. W. Ewers, J. D. Batteas, *Nano Today.* **2015**, *10*, 301.

**ADVANCED
SCIENCE NEWS**

www.advancedsciencenews.com

**ADVANCED
FUNCTIONAL
MATERIALS**

www.afm-journal.de

[62] M. Seol, S. Kim, Y. Cho, K. E. Byun, H. Kim, J. Kim, S. K. Kim, S. W. Kim, H. J. Shin, S. Park, *Adv. Mater.* **2018**, *30*, 1801210.

[63] D.-S. Liu, H. Ryu, U. Khan, C. Wu, J.-H. Jung, J. Wu, Z. Wang, S.-W. Kim, *Nano Energy.* **2021**, *81*, 2211.

[64] Y. Li, Y. Yang, X. Liu, C. Chen, C. Qian, L. Han, Q. Han, *Colloids Surf. A.* **2021**, *628*, 127336.

[65] R. M. Habibur, U. Yaqoob, S. Muhammad, A. S. M. I. Uddin, H. C. Kim, *Mater. Chem. Phys.* **2018**, *215*, 46.

[66] C. Cho, P. Kang, A. Taqieddin, Y. Jing, K. Yong, J. M. Kim, M. F. Haque, N. R. Aluru, S. Nam, *Nat Electron.* **2021**, *4*, 126.

[67] K. Zhang, J. Sun, J. Song, C. Gao, Z. Wang, C. Song, Y. Wu, Y. Liu, *ACS Appl. Mater. Interfaces.* **2020**, *12*, 45306.

[68] Y. Liu, J. Zhong, E. Li, H. Yang, X. Wang, D. Lai, H. Chen, T. Guo, *Nano Energy.* **2019**, *60*, 377.

[69] R. Wen, J. Guo, A. Yu, J. Zhai, Z. l. Wang, *Adv. Funct. Mater.* **2019**, *29*, 1807655.

[70] A. Sett, T. Rana, U. Rajaji, R. Sha, T.-Y. Liu, T. K. Bhattacharyya, *Sens. Actuators, A.* **2022**, *338*, 113507.

[71] L. Zhai, S. Cui, B. Tong, W. Chen, Z. Wu, C. Soutis, D. Jiang, G. Zhu, L. Mi, *Chemistry.* **2020**, *26*, 5784.

[72] T. Ohta, A. Bostwick, T. Seyller, K. Horn, E. Rotenberg, *Science.* **2006**, *313*, 951.

[73] S.-Y. Xia, Y. Long, Z. Huang, Y. Zi, L.-Q. Tao, C.-H. Li, H. Sun, J. Li, *Nano Energy.* **2022**, *96*, 107099.

[74] M. G. Stanford, J. T. Li, Y. Chyan, Z. Wang, W. Wang, J. M. Tour, *ACS Nano.* **2019**, *13*, 7166.

[75] Y. Tang, H. Zhou, X. Sun, N. Diao, J. Wang, B. Zhang, C. Qin, E. Liang, Y. Mao, *Adv. Funct. Mater.* **2019**, *30*, 7893.

[76] D. Zhang, K. Zhang, Y. Wang, Y. Wang, Y. Yang, *Nano Energy.* **2019**, *56*, 25.

[77] Z. Yan, L. Wang, Y. Xia, R. Qiu, W. Liu, M. Wu, Y. Zhu, S. Zhu, C. Jia, M. Zhu, R. Cao, Z. Li, X. Wang, *Adv. Funct. Mater.* **2021**, *31*, 709.

[78] Y. Lee, J. Kim, B. Jang, S. Kim, B. K. Sharma, J.-H. Kim, J.-H. Ahn, *Nano Energy.* **2019**, *62*, 259.

[79] S. K. Karan, R. Bera, S. Paria, A. K. Das, S. Maiti, A. Maitra, B. B. Khatua, *Adv. Energy Mater.* **2016**, *6*, 1601016.

[80] C. Zhu, L.-Q. Tao, Y. Wang, K. Zheng, J. Yu, L. Xiandong, X. Chen, Y. Huang, *Sens. Actuators, B.* **2020**, *325*, 128790.

[81] Z. Wang, J. Chang, Q. Hu, H. Zhi, L. Feng, *Sens. Actuators, B.* **2021**, *345*, 308.

[82] T. K. Sinha, S. K. Ghosh, R. Maiti, S. Jana, B. Adhikari, D. Mandal, S. K. Ray, *ACS Appl. Mater. Interfaces.* **2016**, *8*, 14986.

[83] Y. Meng, J. Zhao, X. Yang, C. Zhao, S. Qin, J. H. Cho, C. Zhang, Q. Sun, Z. L. Wang, *ACS Nano.* **2018**, *12*, 9381.

[84] L. Li, Y. Cheng, H. Cao, Z. Liang, Z. Liu, S. Yan, L. Li, S. Jia, J. Wang, Y. Gao, *Nano Energy.* **2022**, *95*, 986.

[85] D. Zhang, Q. Mi, D. Wang, T. Li, *Sens. Actuators, B.* **2021**, *339*, 923.

[86] Z. Zhang, Q. Yan, Z. Liu, X. Zhao, Z. Wang, J. Sun, Z. L. Wang, R. Wang, L. Li, *Nano Energy.* **2021**, *88*, 6257.

[87] S. K. Karan, D. Mandal, B. B. Khatua, *Nanoscale.* **2015**, *7*, 10655.

[88] Y. Yang, Z. Cao, P. He, L. Shi, G. Ding, R. Wang, J. Sun, *Nano Energy.* **2019**, *66*, 4134.

[89] Y.-W. Cai, X.-N. Zhang, G.-G. Wang, G.-Z. Li, D.-Q. Zhao, N. Sun, F. Li, H.-Y. Zhang, J.-C. Han, Y. Yang, *Nano Energy.* **2021**, *81*, 105663.

[90] X. Zhang, Z. Zhang, Z. Zhou, *J. Energy Chem.* **2018**, *27*, 73.

[91] L. Yang, H. Wang, W. Yuan, Y. Li, P. Gao, N. Tiwari, X. Chen, Z. Wang, G. Niu, H. Cheng, *ACS Appl. Mater. Interfaces.* **2021**, *13*, 60531.

[92] S. Lee, E. H. Kim, S. Yu, H. Kim, C. Park, S. W. Lee, H. Han, W. Jin, K. Lee, C. E. Lee, J. Jang, C. M. Koo, C. Park, *ACS Nano.* **2021**, *15*, 8940.

[93] Y. Yue, N. Liu, W. Liu, M. Li, Y. Ma, C. Luo, S. Wang, J. Rao, X. Hu, J. Su, Z. Zhang, Q. Huang, Y. Gao, *Nano Energy.* **2018**, *50*, 79.

[94] D. Wang, D. Zhang, Y. Yang, Q. Mi, J. Zhang, L. Yu, *ACS Nano.* **2021**, *15*, 2911.

[95] Y. Yang, L. Shi, Z. Cao, R. Wang, J. Sun, *Adv. Funct. Mater.* **2019**, *29*, 7882.

[96] Y. Cao, Y. Guo, Z. Chen, W. Yang, K. Li, X. He, J. Li, *Nano Energy.* **2022**, *92*, 106689

[97] A. Neto, F. Guinea, N. Peres, KS. Novoselov, AK. Geim, *Rev. Mod. Phys.* **2007**, *81*, 1163.

[98] J. Zhu, Y. Zhu, W. Song, H. Wang, M. Gao, M. Cho, I. Park, *ACS Appl. Mater. Interfaces.* **2018**, *10*, 19940.

[99] J. Zhong, Q. Zhong, F. Fan, Y. Zhang, S. Wang, B. Hu, Z. L. Wang, J. Zhou, *Nano Energy.* **2013**, *2*, 491.

[100] A. Neto, F. Guinea, N. Peres, KS. Novoselov, AK. Geim, *Rev. Mod. Phys.* **2007**, *81*, 1163.

[101] G. da Cunha Rodrigues, P. Zelenovskiy, K. Romanyuk, S. Luchkin, Y. Kopelevich, A. Kholkin, *Nat. Commun.* **2015**, *6*, 7572.

[102] G. Zhang, H. Liu, J. Qu, J. Li, *Energy Environ. Sci.* **2016**, *9*, 1190.

[103] K. F. Mak, K. He, J. Shan, TF. Heinz, *Nat. Nanotechnol.* **2012**, *7*, 494.

[104] A. Molina-Sánchez, K. Hummer, L. Wirtz, *Surf. Sci. Rep.* **2015**, *70*, 554.

[105] S. Wang, *Chin. Sci. Bull.* **2016**, *27*, 1225.

[106] T. Cao, G. Wang, W. Han, H. Ye, C. Zhu, J. Shi, Q. Niu, P. Tan, E. Wang, B. Liu, J. Feng, *Nat. Commun.* **2012**, *3*, 887.

[107] H. Nengjie, T. Sefaattin, G. Wenli, L. Renxiong, F. Chao, *Adv. Electron. Mater.* **2015**, *1*, 5.

[108] J.-H. Lin, Y.-H. Tsao, M.-H. Wu, T.-M. Chou, Z.-H. Lin, J. M. Wu, *Nano Energy.* **2017**, *31*, 575.

[109] C. Wu, T. W. Kim, J. H. Park, H. An, J. Shao, X. Chen, Z. L. Wang, *ACS Nano.* **2017**, *11*, 8356.

[110] M. Kim, S. H. Kim, M. U. Park, C. Lee, M. Kim, Y. Yi, K.-H. Yoo, *Nano Energy.* **2019**, *65*, 4079.

[111] S. Park, J. Park, Y.-g. Kim, S. Bae, T.-W. Kim, K.-I. Park, B. H. Hong, C. K. Jeong, S.-K. Lee, *Nano Energy.* **2020**, *78*, 105266.

[112] K. Zhao, W. Sun, X. Zhang, J. Meng, M. Zhong, L. Qiang, M.-J. Liu, B.-N. Gu, C.-C. Chung, M. Liu, F. Yu, Y.-L. Chueh, *Nano Energy.* **2022**, *91*, 6649.

[113] Q. Li, F. Su, G. Tang, X. Xu, Y. Chen, J. Sun, *Tribology Int.* **2022**, *172*, 107590.

[114] N. Gaonkar, R. G. Vaidya, *Phys. E.* **2021**, *128*, 114579.

[115] L. Zhang, Z.-J. Wang, B. Ma, X.-Y. Li, Y.-C. Dai, G. Hu, Y. Peng, Q. Wang, H.-L. Zhang, *Chin. Chem. Lett.* **2021**, *35*, 1001.

[116] G. Wang, Z. Guo, C. Chen, W. Yu, B. Xu, B. Lin, *Sol. Energy.* **2022**, *236*, 576.

[117] X. Chen, Y. Wu, Z. Wu, Y. Han, S. Xu, L. Wang, W. Ye, T. Han, Y. He, Y. Cai, N. Wang, *Nat. Commun.* **2015**, *6*, 7315.

[118] M. Afzaal, P. O'Brien, *Compr. Inorg. Chem. II.* **2013**, *1*, 1001.

[119] L. Li, M. Wu, *Nano Energy.* **2021**, *83*, 105786.

[120] M. Y. Lu, J. Song, M. P. Lu, C. Y. Lee, L. J. Chen, Z. L. Wang, *ACS Nano.* **2009**, *3*, 357.

[121] Y. Qian, J. Yu, F. Zhang, Y. Kang, C. Su, H. Pang, *Nano Energy.* **2021**, *88*, 106256.

[122] S. Mishra, S. Potu, R. S. Puppala, R. K. Rajaboina, P. Kodali, H. Divi, *Mat. Tod. Comm.* **2022**, *31*, 292.

[123] S. Mishra, P. Supraja, P. R. Sankar, R. R. Kumar, K. Prakash, D. Haranath, *Mater. Chem. Phys.* **2022**, *277*, 125264.

[124] M. K. Gupta, J. H. Lee, K. Y. Lee, SW. Kim, *ACS Nano.* **2013**, *7*, 8932.

[125] B. Yin, Y. Qiu, H. Zhang, J. Lei, Y. Chang, J. Ji, Y. Luo, Y. Zhao, L. Hu, *Nano Energy.* **2015**, *14*, 95.

[126] Z. You, S. Wang, Z. Li, Y. Zou, T. Lu, F. Wang, B. Hu, X. Wang, L. Li, W. Fang, Y. Liu, *Nano Energy.* **2022**, *91*, 106667.

**ADVANCED
SCIENCE NEWS**

www.advancedsciencenews.com

**ADVANCED
FUNCTIONAL
MATERIALS**

www.afm-journal.de

[127] P. Bhat, P. Salunkhe, M. S. Murari, D. Kekuda, *Sens. Actuators, A.* **2022**, *338*, 113479.

[128] S. Sardana, H. Kaur, B. Arora, D. K. Aswal, A. Mahajan, *ACS Sens.* **2022**, *7*, 312.

[129] X. Wu, *Opt. Commun.* **2018**, *425*, 172.

[130] P. Zhao, G. Bhattacharya, S. J. Fishlock, J. G. M. Guy, A. Kumar, C. Tsonos, Z. Yu, S. Raj, J. A. McLaughlin, J. Luo, N. Soin, *Nano Energy.* **2020**, *75*, 4958.

[131] Y. Dai, X. Wang, W. Peng, C. Wu, Y. Ding, K. Dong, Z. L. Wang, *Nano Energy.* **2018**, *44*, 311.

[132] Z. Gao, W. Jin, Y. Zhou, Y. Dai, B. Yu, C. Liu, W. Xu, Y. Li, H. Peng, Z. Liu, L. Dai, *Nanoscale.* **2013**, *5*, 5576.

[133] Y. Peng, J. Lu, X. Wang, W. Ma, M. Que, Q. Chen, F. Li, X. Liu, W. Gao, C. Pan, *Nano Energy.* **2022**, *94*, 106945.

[134] Y. Q. Bie, Z. M. Liao, H. Z. Zhang, G. R. Li, Y. Ye, Y. B. Zhou, J. Xu, Z. X. Qin, L. Dai, D. P. Yu, *Adv. Mater.* **2011**, *23*, 649.

[135] K.-A. N. Duerloo, M. T. Ong, E. J. Reed, *J. Phys. Chem. Lett.* **2012**, *3*, 2871.

[136] H. Song, I. Karakurt, M. Wei, N. Liu, Y. Chu, J. Zhong, L. Lin, *Nano Energy.* **2018**, *49*, 7.

[137] J.-H. Lee, J. Y. Park, E. B. Cho, T. Y. Kim, S. A. Han, T.-H. Kim, Y. Liu, S. K. Kim, C. J. Roh, H.-J. Yoon, H. Ryu, W. Seung, J. S. Lee, J. Lee, S.-W. Kim, *Adv. Mater.* **2017**, *29*, 6667.

[138] Q. Zhang, T. Jiang, D. Ho, S. Qin, X. Yang, J. H. Cho, Q. Sun, Z. L. Wang, *ACS Nano.* **2018**, *12*, 254.

[139] J. Zhao, Z. Wei, Q. Zhang, H. Yu, S. Wang, X. Yang, G. Gao, S. Qin, G. Zhang, Q. Sun, Z. L. Wang, *ACS Nano.* **2018**, *13*, 582.

[140] K. Roy, M. Padmanabhan, S. Goswami, T. P. Sai, G. Ramalingam, S. Raghavan, A. Ghosh, *Nat. Nanotechnol.* **2013**, *8*, 826.

[141] S. Xu, L. Guo, Q. Sun, Z. L. Wang, *Adv. Funct. Mater.* **2019**, *29*, 8737.

[142] J. Jiang, J. Guo, X. Wan, Y. Yang, H. Xie, D. Niu, J. Yang, J. He, Y. Gao, Q. Wan, *Small.* **2017**, *13*, 4506.

[143] X. Yang, J. Yu, J. Zhao, Y. Chen, G. Gao, Y. Wang, Q. Sun, Z. L. Wang, *Adv. Funct. Mater.* **2020**, *30*, 2506.

[144] S. Qin, Q. Zhang, X. Yang, M. Liu, Q. Sun, Z. L. Wang, *Adv. Energy Mater.* **2018**, *8*, 23.

[145] G. Gao, J. Yu, X. Yang, Y. Pang, J. Zhao, C. Pan, Q. Sun, Z. L. Wang, *Adv. Mater.* **2019**, *31*, 6905.

[146] J. Yu, G. Gao, J. Huang, X. Yang, J. Han, H. Zhang, Y. Chen, C. Zhao, Q. Sun, Z. L. Wang, *Nat Commun.* **2021**, *12*, 1581.

[147] F. Tan, Y. Xiong, J. Yu, Y. Wang, Y. Li, Y. Wei, J. Sun, X. Xie, Q. Sun, Z. L. Wang, *Nano Energy.* **2021**, *90*, 6617.

[148] X. Yang, J. Han, J. Yu, Y. Chen, H. Zhang, M. Ding, C. Jia, J. Sun, Q. Sun, Z. L. Wang, *ACS Nano.* **2020**, *14*, 8668.

[149] Z. Lou, S. Chen, L. Wang, K. Jiang, G. Shen, *Nano Energy.* **2016**, *23*, 7.

[150] X. Fu, L. Wang, L. Zhao, Z. Yuan, Y. Zhang, D. Wang, D. Wang, J. Li, D. Li, V. Shulga, G. Shen, W. Han, *Adv. Funct. Mater.* **2021**, *31*, 533.

[151] Y. Wang, L. Wang, T. Yang, X. Li, X. Zang, M. Zhu, K. Wang, D. Wu, H. Zhu, *Adv. Funct. Mater.* **2014**, *24*, 4666.

[152] K. Roy, S. K. Ghosh, A. Sultana, S. Garain, M. Xie, C. R. Bowen, K. Henkel, D. Schmeißer, D. Mandal, *ACS Appl. Nano Mater.* **2019**, *2*, 2013.

[153] J. Huang, Y. Hao, M. Zhao, W. Li, F. Huang, Q. Wei, *ACS Appl. Mater. Interfaces.* **2021**, *13*, 24774.

[154] J. Gu, Y. Peng, T. Zhou, J. Ma, H. Pang, Y. Yamauchi, *Nano Res. Energy.* **2022**, *1*, e9120009.

[155] M. Salauddin, S. M. S. Rana, M. T. Rahman, M. Sharifuzzaman, P. Maharjan, T. Bhatta, H. Cho, S. H. Lee, C. Park, K. Shrestha, S. Sharma, J. Y. Park, *Adv. Funct. Mater.* **2021**, *32*, 1840.

[156] F.-R. Fan, Z.-Q. Tian, Z. Lin Wang, *Nano Energy.* **2012**, *1*, 328.

[157] S. Rana, V. Singh, B. Singh, *iScience.* **2022**, *25*, 103748.

[158] M. Faraz, H. H. Singh, N. Khare, *J. Alloys Comp.* **2022**, *890*, 161840.

[159] B. Saravanakumar, S.-J. Kim, *J. Phys. Chem. C.* **2014**, *118*, 8831.

[160] N. Kaur, J. Bahadur, V. Panwar, P. Singh, K. Rathi, K. Pal, *Sci. Rep.* **2016**, *6*, 38835.

[161] S. K. Kim, R. Bhatia, T.-H. Kim, D. Seol, J. H. Kim, H. Kim, W. Seung, Y. Kim, Y. H. Lee, S.-W. Kim, *Nano Energy.* **2016**, *22*, 483.

[162] L. Feng, G. Liu, H. Guo, Q. Tang, X. Pu, J. Chen, X. Wang, Y. Xi, C. Hu, *Nano Energy.* **2018**, *47*, 217.

[163] N. R. Hemanth, B. Kandasubramanian, *Chem. Eng. J.* **2020**, *392*, 123678.

[164] Y. Sun, D. Chen, Z. Liang, *Mater. Tod. Energy.* **2017**, *5*, 22.

[165] N. Fatima, M. B. Tahir, A. Noor, M. Sagir, M. S. Tahir, H. Alrobei, U. Fatima, K. Shahzad, A. M. Ali, S. Muhammad, *Int. J. Hydrogen Energy.* **2021**, *46*, 25413.

[166] S. Karmakar, R. Sarkar, C. S. Tiwary, P. Kumbhakar, *J. Alloys Compd.* **2020**, *844*, 155690.

[167] X. Xia, Q. Liu, Y. Zhu, Y. Zi, *EcoMat.* **2020**, *2*, 258.

[168] J. J. Grant, S. C. Pillai, S. Hehir, M. McAfee, A. Breen, *ACS Biomater Sci Eng.* **2021**, *7*, 1278.

[169] R. Sha, T. K. Bhattacharyya, *Electrochim. Acta.* **2020**, *349*, 136370.

[170] Q. Zheng, B. Shi, Z. Li, Z. L. Wang, *Adv. Sci.* **2017**, *4*, 1700029.

[171] H. Yoon, J. Nah, H. Kim, S. Ko, M. Sharifuzzaman, S. C. Barman, X. Xuan, J. Kim, J. Y. Park, *Sens. Actuators, B.* **2020**, *311*, 127866.

[172] L. Wang, J. Jie, Z. Shao, Q. Zhang, X. Zhang, Y. Wang, Z. Sun, S.-T. Lee, *Adv. Funct. Mater.* **2015**, *25*, 2910.

[173] H. Xue, H. Gong, Y. Yamauchi, T. Sasaki, R. Ma, *Nano Res. Energy.* **2022**, *1*, e9120007.

[174] S. Payandeh, F. Strauss, A. Mazilkin, A. Kondrakov, T. Brezesinski, *Nano Res. Energy.* **2022**, *1*, e9120007.

[175] J. Guo, R. Wen, J. Zhai, Z. L. Wang, *Sci. Bull.* **2019**, *64*, 128.

[176] E. Lee, A. VahidMohammadi, Y. S. Yoon, M. Beidaghi, D. J. Kim, *ACS Sens.* **2019**, *4*, 1603.

[177] J. Z. Ou, W. Ge, B. Carey, T. Daeneke, A. Rotbart, W. Shan, Y. Wang, Z. Fu, A. Chrimes, W. Wlodarski, *ACS Nano.* **2015**, *15*, 10313.

[178] Y. Dai, Y. Xiong, *Nano Res. Energy.* **2022**, *1*, e9120006.

[179] T. Someya, Y. Kato, T. Sekitani, S. Iba, Y. Noguchi, Y. Murase, H. Kawaguchi, T. Sakurai, *Proceedings Nat. Acad. Sci. USA.* **2005**, *102*, 12321.

[180] Y. X. Hou, Y. Li, Z. C. Zhang, J. Q. Li, D. H. Qi, X. D. Chen, J. J. Wang, B. W. Yao, M. X. Yu, T. B. Lu, J. Zhang, *ACS Nano.* **2021**, *15*, 1497.

[181] Y. Lee, J. Park, A. Choe, S. Cho, J. Kim, H. Ko, *Adv. Funct. Mater.* **2019**, *30*, 4523.

[182] S. Gong, W. Schwalb, Y. Wang, Y. Chen, Y. Tang, J. Si, B. Shirinzadeh, W. Cheng, *Nat. Commun.* **2014**, *5*, 3132.

[183] Z. Song, W. Ye, Z. Chen, Z. Chen, M. Li, W. Tang, C. Wang, Z. Wan, S. Poddar, X. Wen, X. Pan, Y. Lin, Q. Zhou, Z. Fan, *ACS Nano.* **2021**, *15*, 7659.

[184] J. Yang, J. Chen, Y. Su, Q. Jing, Z. Li, F. Yi, X. Wen, Z. Wang, Z. L. Wang, *Adv. Mater.* **2015**, *27*, 1316.

[185] X. Han, Z. Xu, W. Wu, X. Liu, P. Yan, C. Pan, *Small Struct.* **2020**, *1*, 2000029.

[186] W. Li, D. Torres, R. Diaz, Z. Wang, C. Wu, C. Wang, Z. Lin Wang, N. Sepulveda, *Nat. Commun.* **2017**, *8*, 15310.

[187] Q. Sun, D. H. Ho, Y. Choi, C. Pan, D. H. Kim, Z. L. Wang, J. H. Cho, *ACS Nano.* **2016**, *10*, 11037.

[188] B. Y. Lee, D. H. Kim, J. Park, K. I. Park, K. J. Lee, C. K. Jeong, *Sci. Technol. Adv. Mater.* **2019**, *20*, 758.

[189] J. Yu, X. Yang, Q. Sun, *Adv. Intell. Syst.* **2020**, *2*, 546.

[190] E. Kar, N. Bose, B. Dutta, S. Banerjee, N. Mukherjee, S. Mukherjee, *Energy Convers. Manage.* **2019**, *184*, 600.

[191] F. Xue, J. Zhang, W. Hu, W. T. Hsu, A. Han, S. F. Leung, J. K. Huang, Y. Wan, S. Liu, J. Zhang, J. H. He, W. H. Chang, Z. L. Wang, X. Zhang, L. J. Li, *ACS Nano.* **2018**, *12*, 4976.

2206900 (28 of 30)

[192] C. Qian, Y. Choi, S. Kim, S. Kim, Y. J. Choi, D. G. Roe, J. H. Lee, M. S. Kang, W. H. Lee, J. H. Cho, *Adv. Funct. Mater.* **2022**, *32*, 2490.

[193] E. Lee, A. VahidMohammadi, B. C. Prorok, Y. S. Yoon, M. Beidaghi, D. J. Kim, *ACS Appl. Mater. Interfaces* **2017**, *9*, 37184.

[194] Y. Cheng, W. Zhu, X. Lu, C. Wang, *Nano Energy.* **2022**, *98*, 229.

[195] Y. Jeong, D. Shin, J. H. Park, J. Park, Y. Yi, S. Im, *Nano Energy.* **2019**, *63*, 103833.

[196] J. K. Han, S. Kim, S. Jang, Y. R. Lim, S.-W. Kim, H. Chang, W. Song, S. S. Lee, J. Lim, K.-S. An, S. Myung, *Nano Energy.* **2019**, *61*, 471.

[197] Y. Cheng, R. Wang, J. Sun, L. Gao, *Adv. Mater.* **2015**, *27*, 7365.

[198] S. Zhang, J. Guo, L. Liu, H. Ruan, C. Kong, X. Yuan, B. Zhang, G. Gu, P. Cui, G. Cheng, Z. Du, *Nano Energy.* **2022**, *91*, 660.

[199] L. Q. Tao, K. N. Zhang, H. Tian, Y. Liu, D. Y. Wang, Y. Q. Chen, Y. Yang, T. L. Ren, *ACS Nano.* **2017**, *11*, 8790.

[200] S. Zhang, L. Sun, Q. Fan, F. Zhang, Z. Wang, J. Zou, S. Zhao, J. Mao, Z. Guo, *Nano Research Energy.* **2022**, *1*, e9120001.

[201] Y. Manjula, R. Rakesh Kumar, P. M. Swarup Raju, G. Anil Kumar, T. Venkatappa Rao, A. Akshaykranth, P. Supraja, *Chem. Phys.* **2020**, *533*, 110699.

[202] R. R. Nair, P. Blake, A. N. Grigorenko, K. S. Novoselov, T. J. Booth, T. Stauber, N. M. Peres, A. K. Geim, *Science.* **2008**, *320*, 1308.

[203] Q. Bao, H. Zhang, Y. Wang, Z. Ni, Y. Yan, Z. X. Shen, K. P. Loh, D. Y. Tang, *Adv. Funct. Mater.* **2009**, *19*, 3077.

[204] Y. Dong, S. S. K. Mallineni, K. Maleski, H. Behlow, V. N. Mochalin, A. M. Rao, Y. Gogotsi, R. Podila, *Nano Energy.* **2018**, *44*, 103.

[205] T. Bhatta, P. Maharjan, H. Cho, C. Park, S. H. Yoon, S. Sharma, M. Salauddin, M. T. Rahman, S. M. S. Rana, J. Y. Park, *Nano Energy.* **2021**, *81*, 105670.

[206] C. Jiang, X. Li, Y. Yao, L. Lan, Y. Shao, F. Zhao, Y. Ying, J. Ping, *Nano Energy.* **2019**, *66*, 104121.

[207] N. Higashitarumizu, H. Kawamoto, C. J. Lee, B. H. Lin, F. H. Chu, I. Yonemori, T. Nishimura, K. Wakabayashi, W. H. Chang, K. Nagashio, *Nat. Commun.* **2020**, *11*, 2428.

[208] G. Gao, B. Wan, X. Liu, Q. Sun, X. Yang, L. Wang, C. Pan, Z. L. Wang, *Adv. Mater.* **2018**, *30*, 5088.

[209] Y. Cheng, Y. Ma, L. Li, M. Zhu, Y. Yue, W. Liu, L. Wang, S. Jia, C. Li, T. Qi, J. Wang, Y. Gao, *ACS Nano.* **2020**, *14*, 2145.

[210] W. He, M. Sohn, R. Ma, D. J. Kang, *Nano Energy.* **2020**, *78*, 105383.

[211] E. Islam, A. M. Abdullah, A. R. Chowdhury, F. Tasnim, M. Martinez, C. Olivares, K. Lozano, M. J. Uddin, *Nano Energy.* **2020**, *77*, 105250.

[212] P. Sahatiya, S. Kannan, S. Badhulika, *Appl. Mater. Today.* **2018**, *13*, 91.

[213] N. Muralidharan, M. Li, R. E. Carter, N. Galioto, C. L. Pint, *ACS Energy Lett.* **2017**, *2*, 1797.

[214] Y. Yang, W. Guo, K. C. Pradel, G. Zhu, Y. Zhou, Y. Zhang, Y. Hu, L. Lin, Z. L. Wang, *Nano Lett.* **2012**, *12*, 2833.

[215] R. Que, Q. Shao, Q. Li, M. Shao, S. Cai, S. Wang, S. T. Lee, *Angew Chem Int Ed Engl.* **2012**, *51*, 5418.

[216] Y. Liu, E. Li, Y. Yan, Z. Lin, Q. Chen, X. Wang, L. Shan, H. Chen, T. Guo, *Nano Energy.* **2021**, *86*, 89.

[217] S. Guo, K. Wu, C. Li, H. Wang, Z. Sun, D. Xi, S. Zhang, W. Ding, M. E. Zaghloul, C. Wang, F. A. Castro, D. Yang, Y. Zhao, *Matter.* **2021**, *4*, 969.

[218] L. Zhao, L. Wang, Y. Zheng, S. Zhao, W. Wei, D. Zhang, X. Fu, K. Jiang, G. Shen, W. Han, *Nano Energy.* **2021**, *84*, 106118.

[219] H. Seo, S. I. Han, K. I. Song, D. Seong, K. Lee, S. H. Kim, T. Park, J. H. Koo, M. Shin, H. W. Baac, O. K. Park, S. J. Oh, H. S. Han, H. Jeon, Y. C. Kim, D. H. Kim, T. Hyeon, D. Son, *Adv. Mater.* **2021**, *33*, 2007346.

[220] Y. Yao, J. Chen, Y. Guo, T. Lv, Z. Chen, N. Li, S. Cao, B. Chen, T. Chen, *Biosens. Bioelectron.* **2021**, *179*, 113078.

[221] J. Yang, K. Zhang, J. Yu, S. Zhang, L. He, S. Wu, C. Liu, Y. Deng, *Adv. Mater. Technol.* **2021**, *33*, 7346.

[222] D. Zhang, Z. Xu, Z. Yang, X. Song, *Nano Energy.* **2020**, *67*, 158.

[223] X. Wang, D. Zhang, H. Zhang, L. Gong, Y. Yang, W. Zhao, S. Yu, Y. Yin, D. Sun, *Nano Energy.* **2021**, *88*, 262.

[224] D. Zhang, Z. Yang, P. Li, M. Pang, Q. Xue, *Nano Energy.* **2019**, *67*, 4251.

[225] Y. Fu, W. Zang, P. Wang, L. Xing, X. Xue, Y. Zhang, *Nano Energy.* **2014**, *8*, 34.

[226] X. Ma, C. Wang, R. Wei, J. He, J. Li, X. Liu, F. Huang, S. Ge, J. Tao, Z. Yuan, P. Chen, D. Peng, C. Pan, *ACS Nano.* **2022**, *16*, 2789.

[227] P.-K. Yang, S.-A. Chou, C.-H. Hsu, R. J. Mathew, K.-H. Chiang, J.-Y. Yang, Y.-T. Chen, *Nano Energy.* **2020**, *75*, 96.

[228] C. G. Núñez, W. T. Navaraj, E. O. Polat, R. Dahiya, *Adv. Funct. Mater.* **2017**, *27*, 1606287.

[229] S. Hong, N. Zagni, S. Choo, N. Liu, S. Baek, A. Bala, H. Yoo, B. H. Kang, H. J. Kim, H. J. Yun, M. A. Alam, S. Kim, *Nat Commun.* **2021**, *12*, 3559.

[230] J. Yu, X. Yang, G. Gao, Y. Xiong, Z. L. Wang, *Sci. Adv.* **2021**, *7*, 9117.

Ziwei Huo received her bachelor's degree from the College of Electric and Electrical Engineering, Henan Normal University, in 2021. Now she is a master's candidate at the Beijing Institute of Nanoenergy and Nanosystems, Chinese Academy of Sciences. Her main research interests include self-powered sensors, wearable electronics, and intelligent applications based on triboelectric nanogenerators.

**ADVANCED
SCIENCE NEWS**

www.advancedsciencenews.com

**ADVANCED
FUNCTIONAL
MATERIALS**

www.afm-journal.de

Yichen Wei received his Master's degree from Dalian Polytechnic University in 2019. He is a Ph.D. candidate at the School of Physical Science and Technology, Guangxi University. His research focuses on tribotronic two-dimension semiconductor FETs and extended applications in neuromorphic computation.

Yifei Wang received his B.S. degree from the School of Materials Science and Engineering, China University of Geosciences (Beijing). He is pursuing his Ph.D. under the supervision of Professor Qijun Sun at Beijing Institute of Nanoenergy and Nanosystems, Chinese Academy of Sciences, University of Chinese Academy of Sciences. His current research interests are focused on tribo-electric nanogenerators and novel neuromorphic devices.

Zhong Lin Wang received his Ph. D from Arizona State University in physics. He now is the Hightower Chair in Materials Science and Engineering, Regents' Professor, Engineering Distinguished Professor, and Director, Center for Nanostructure Characterization at Georgia Tech. Dr. Wang has made original and innovative contributions to the synthesis, discovery, characterization and understanding of fundamental physical properties of oxide nanobelts and nanowires, as well as applications of nanowires in energy sciences, electronics, optoelectronics, and biological science. He pioneered the field of piezotronics and piezo-phototronics by introducing piezoelectric potential gated charge transport process in fabricating new electronic and optoelectronic devices.
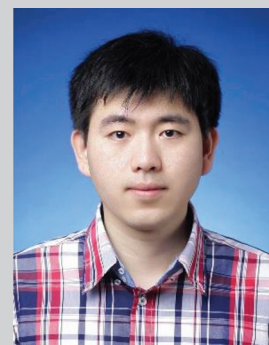
Qijun Sun received his Ph. D from Gachon University in 2013. He worked as a postdoctoral researcher in POSTECH and SKKU from 2013 to 2015. Since 2016, he has joined the Beijing Institute of Nanoenergy and Nanosystems, CAS, as the principal investigator of the Functional Soft Electronics Lab. The main research interests of his group include triboiontronic devices, mechanoplastic neuromorphic transistors, artificial synaptic devices electronic skin, 2D materials-based flexible semiconductor devices, human-machine interactive systems, and micro-nano fabrication, aiming to develop advanced systems for human health monitoring and human-robotic interface.